UCSF
UC San Francisco Previously Published Works

Title
GPR35 promotes neutrophil recruitment in response to serotonin metabolite 5-HIAA

Permalink
https://escholarship.org/uc/item/4vz6r1bh

Journal
Cell, 185(6)

ISSN
0092-8674

Authors
De Giovanni, Marco
Tam, Hanson
Valet, Colin
et al.

Publication Date
2022-03-01

DOI
10.1016/j.cell.2022.03.003

Peer reviewed

eScholarship.org Powered by the California Digital Library
University of California

Cell

Article

GPR35 promotes neutrophil recruitment in response to serotonin metabolite 5-HIAA

Graphical abstract

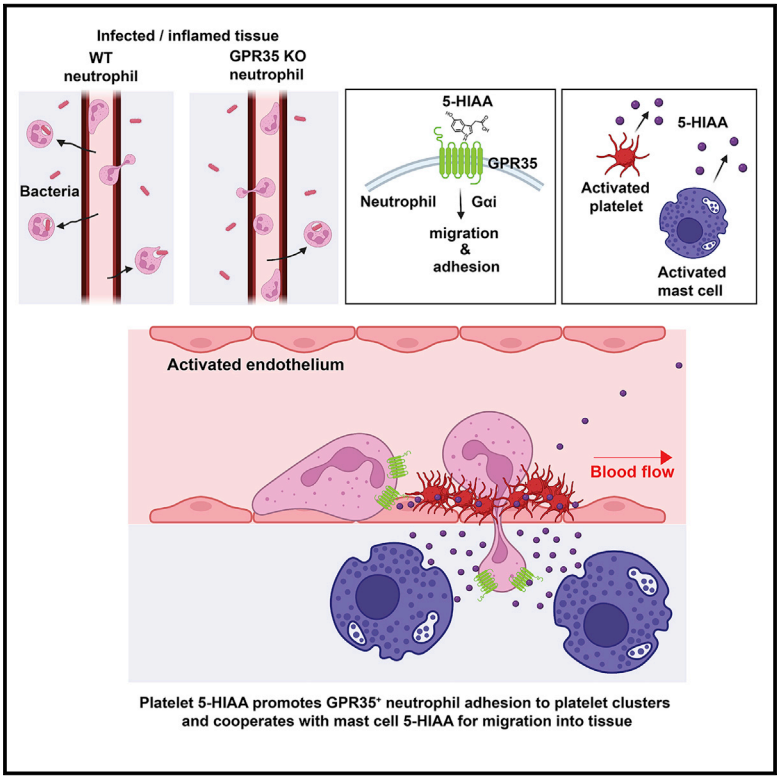

Highlights

- GPR35 upregulation on activated neutrophils helps in inflammatory recruitment
- Serotonin metabolite 5-hydroxyindoleacetic acid (5-HIAA) acts as a GPR35 ligand
- Platelet- and mast cell-derived 5-HIAA promote neutrophil transendothelial migration
- Inhibitors of serotonin reuptake and metabolism diminish GPR35 function

Authors

Marco De Giovanni, Hanson Tam, Colin Valet, Ying Xu, Mark R. Looney, Jason G. Cyster

Correspondence

marco.degiovanni@ucsf.edu (M.D.G.), jason.cyster@ucsf.edu (J.G.C.)

In brief

Platelet- and mast-cell-derived 5-HIAA is a ligand of GPR35 that promotes neutrophil transendothelial migration and recruitment to sites of inflammation upon bacterial infection.

De Giovanni et al., 2022, Cell *185*, 815–830
March 3, 2022 © 2022 Elsevier Inc.
https://doi.org/10.1016/j.cell.2022.01.010

CellPress

Cell

CellPress

Article

GPR35 promotes neutrophil recruitment in response to serotonin metabolite 5-HIAA

Marco De Giovanni,[1,*] Hanson Tam,[1] Colin Valet,[2] Ying Xu,[1] Mark R. Looney,[2] and Jason G. Cyster[1,3,*]

[1]Howard Hughes Medical Institute, Department of Microbiology and Immunology, University of California, San Francisco, San Francisco, CA 94143, USA

[2]Departments of Medicine and Laboratory Medicine, University of California, San Francisco, San Francisco, CA 94143, USA

[3]Lead contact

*Correspondence: marco.degiovanni@ucsf.edu (M.D.G.), jason.cyster@ucsf.edu (J.G.C.)

https://doi.org/10.1016/j.cell.2022.01.010

SUMMARY

Rapid neutrophil recruitment to sites of inflammation is crucial for innate immune responses. Here, we reveal that the G-protein-coupled receptor GPR35 is upregulated in activated neutrophils, and it promotes their migration. GPR35-deficient neutrophils are less recruited from blood vessels into inflamed tissue, and the mice are less efficient in clearing peritoneal bacteria. Using a bioassay, we find that serum and activated platelet supernatant stimulate GPR35, and we identify the platelet-derived serotonin metabolite 5-hydroxyindoleacetic acid (5-HIAA) as a GPR35 ligand. GPR35 function in neutrophil recruitment is strongly dependent on platelets, with the receptor promoting transmigration across platelet-coated endothelium. Mast cells also attract GPR35^{+} cells via 5-HIAA. Mice deficient in 5-HIAA show a loss of GPR35-mediated neutrophil recruitment to inflamed tissue. These findings identify 5-HIAA as a GPR35 ligand and neutrophil chemoattractant and establish a role for platelet- and mast cell-produced 5-HIAA in cell recruitment to the sites of inflammation and bacterial clearance.

INTRODUCTION

Neutrophils are crucial early responders at sites of inflammation, mediating rapid clearance of invading bacteria, and defects in neutrophil recruitment are a cause of recurrent infections in humans (Etzioni, 2009). Neutrophil recruitment to the sites of inflammation occurs via a multistep cascade (Nourshargh and Alon, 2014). Locally, the endothelium upregulates selectins and integrin ligands, whereas, systemically, neutrophils are mobilized from the bone marrow (BM) (Strydom and Rankin, 2013). Mobilized neutrophils highly express molecules needed for homing, including P-selectin glycoprotein ligand-1, chemokine receptors, and integrins. Neutrophils enter into rolling interactions with selectin-expressing endothelium, allowing encounter with chemokines displayed on the endothelium that can then trigger firm integrin-mediated adhesion and crawling (Nourshargh and Alon, 2014). Multiple additional signals subsequently promote transendothelial migration, and the precise requirements for this step continue to be determined (Filippi, 2019; Girbl et al., 2018).

Activated platelets can rapidly adhere to the inflamed endothelium and display P-selectin and integrin ligands, providing additional support for neutrophil attachment (Deppermann and Kubes, 2018; Maas et al., 2018). Platelets also release granules containing numerous mediators, including chemokines and lipids that promote neutrophil adhesion and transmigration steps (Deppermann and Kubes, 2018; Maas et al., 2018; Rossaint et al., 2016). Platelets contribute to neutrophil recruitment to inflamed peritoneum, lymph nodes (LNs), skin, and other sites (Bogoslowski et al., 2018; Deppermann and Kubes, 2018; Gros et al., 2015; Kornerup et al., 2010; Maas et al., 2018; Zarbock et al., 2006). Another cell type that contributes to neutrophil recruitment is the perivascular mast cell. Mast cells can be activated by a range of inflammatory agents, and they promptly release multiple mediators that contribute to mobilizing selectins on endothelial cells, promoting vascular leakiness and chemoattracting neutrophils (Galli et al., 2020; Wernersson and Pejler, 2014). There is evidence for platelet-mast cell communication across the endothelium, such that activation of one cell type can cause activation of the other (Karhausen et al., 2020; Schwartz, 1987).

The G-protein-coupled receptor (GPCR) GPR35 is expressed by various myeloid cell types, as well as by intestinal epithelium, peripheral sensory neurons, adipose, and cardiovascular tissue (Quon et al., 2020). Ligand screening studies have identified multiple candidate ligands for GPR35, the most studied being kynurenic acid (KynA), as well as several synthetic agonists, including Lodoximide (Deng et al., 2012; Foata et al., 2020; Taniguchi et al., 2006; Wang et al., 2006; Zhao et al., 2010). Lysophosphatidic acid (LPA) has also been suggested to be a GPR35 ligand, with 2-acyl LPA being more active (Kaya et al., 2020; Oka et al., 2010). However, the low (micromolar) potency of the identified ligands has led to the view that GPR35 remains an orphan receptor (Quon et al., 2020). In some studies, GPR35 was reported to couple to $G\alpha_{12}/G\alpha_{13}$ and support Rho activation (Jenkins et al., 2011; Mackenzie et al., 2019; Park et al., 2018) and

thus possible migration inhibition, whereas in other cases, it was found to couple to $G\alpha_i$ family members and promote chemotactic migration (Agudelo et al., 2018; Barth et al., 2009; Ohshiro et al., 2008; Taniguchi et al., 2006). An *in vitro* study reported that GPR35 agonism with KynA can promote arrest of monocytes and neutrophils on endothelium under flow conditions (Barth et al., 2009). However, whether GPR35 mediates neutrophil chemoattraction or recruitment to sites of inflammation *in vivo* is not known.

Here, we set out to define the significance of GPR35 expression in neutrophils in the context of their trafficking to sites of inflammation and to define ligand requirements for GPR35 function. We found that GPR35 was rapidly upregulated on mobilized neutrophils and that it supported their chemotactic migration. *In vivo*, GPR35 contributed to the efficiency of neutrophil recruitment to three sites of inflammation and augmented clearance of bacteria from the peritoneum. Using a bioassay, serum and activated platelet supernatant were found to engage GPR35, and we identified the platelet-derived metabolite 5-hydroxyindoleacetic acid (5-HIAA) as a nanomolar GPR35 ligand. Platelets were important for GPR35-mediated neutrophil recruitment, and imaging experiments showed GPR35 augmented neutrophil transmigration in regions of platelet accumulation. Mast cells, another source of 5-HIAA, contributed to the GPR35-dependent neutrophil recruitment.

Treatment with serotonin uptake inhibitor fluoxetine to prevent platelet loading with serotonin or with a monoamine oxidase (MAO) inhibitor to block conversion of serotonin to 5-HIAA overcame GPR35-mediated neutrophil recruitment. Genetic deficiency in the serotonin transporter (SERT) in platelets or of the serotonin biosynthetic enzyme tryptophan hydroxylase-1 (Tph1) in hematopoietic cells also caused loss of GPR35-dependent recruitment. The findings establish GPR35–5-HIAA as a chemoattractant receptor–ligand system that cooperates with other inflammation-induced factors in mediating neutrophil recruitment to sites of inflammation. In addition, given GPR35 expression across diverse cell types, these data shed light on 5-HIAA as an inflammatory mediator for immune and non-immune cell populations.

RESULTS

GPR35 expression and pro-migratory activity in neutrophils

Acute peritonitis represents a serious medical condition, and rapid neutrophil recruitment is essential for protection against invading peritoneal pathogens (Buscher et al., 2016). In the thioglycolate (TG) model of peritonitis, there is strong neutrophil recruitment to the peritoneum that begins in the first hours after TG injection and persists for at least 24 h (Ajuebor et al., 1999). In a time-course experiment, *Gpr35* was more than 10-fold upregulated in peritoneal neutrophils at 2 h and expression had begun to decline by 18 h (Figure 1A). *Gpr35* expression in blood neutrophils was higher than in immature BM neutrophils and was upregulated after 2 h of mobilization (Figure 1A). Staining for total GPR35 protein with an antibody against the C-terminal cytoplasmic domain confirmed that protein expression was strongly upregulated within 2 h (Figure 1B). Subcutaneous *Listeria monocytogenes* inoculation also led to the upregulation of *Gpr35* in neutrophils recruited to the draining LNs, whereas skin pricking with a *Listeria*-contaminated needle led to the GPR35 upregulation in neutrophils recruited to skin (Figures S1A and S1B). Analysis of a scRNA-seq dataset (Xie et al., 2020) showed that *Gpr35* expression was elevated in neutrophils recruited to the peritoneum in response to *E. coli* while being minimally expressed in BM neutrophils (Figures S1C and S1D). In gene expression data from human neutrophils exposed to the gram-negative bacterium *Francisella tularensis* (Schwartz et al., 2013), GPR35 was strongly upregulated at 6 h (Figure S1E).

In experiments with GPR35 transfected WEHI-231 B lymphoma cells, GPR35-dependent chemotactic responses were detected to micromolar amounts of Lodoxamide and KynA but not to 1-acyl or 2-acyl LPA (Figures 1C, 1D, S1F, and S1G). Migration could be inhibited by pertussis toxin (PTX) treatment, in accord with chemotactic migration depending on $G\alpha_i$-coupling (Figure S1H). Additionally, Lodoxamide and high micromolar amounts of KynA—but not LPA—were effective at promoting internalization of GPR35 (Figures S1I–S1K). Mobilized neutrophils were also found to transmigrate across an endothelial monolayer to millimolar amounts of KynA in a GPR35-dependent manner (Figures 1E and 1F). In accord with previous work (Barth et al., 2009), KynA could promote adhesion of $GPR35^+$ cells to an endothelial monolayer in an integrin-dependent manner (Figures 1G and S1L). These findings demonstrated that GPR35 could function as a pro-migratory and pro-adhesive receptor in mobilized neutrophils, although, as with findings in other contexts (Barth et al., 2009; Quon et al., 2020), the high amounts of KynA required for these actions made it unlikely that it was a physiological ligand.

GPR35 promotes neutrophil recruitment to sites of inflammation

The ability of GPR35 to support *in vitro* migration of mobilized neutrophils suggested that it may influence their recruitment to sites of inflammation. Using a mixed transfer approach in mice, GPR35-deficiency led to a 2-fold reduction in neutrophil recruitment to the inflamed peritoneum at 18 h after TG injection (Figures 2A, 2B, S2A, and S2B). Time course studies showed that GPR35 KO cell homing was already reduced at 2 h after TG treatment (Figure S2C). Similar findings were obtained for peritoneal homing of endogenous neutrophils in TG immunized GPR35 WT:KO mixed BM chimeras that contain approximately equal frequencies of WT- and GPR35-deficient neutrophils (Figure S2D) and also in full GPR35 KO mice (Figures S2E and S2F). In peritoneally inflamed GPR35 KO mice, there was an increased frequency of neutrophils in the blood, which is likely a consequence of the reduced peritoneal recruitment (Figures S2G and S2H). Total cell numbers in the inflamed peritoneum were not affected by GPR35-deficiency, indicating selectivity in the neutrophil recruitment defect (Figure S2I). GPR35-deficient neutrophil recruitment to the peritoneum was also reduced following TNF-induced inflammation (Figure 2C). Deficiency in IDO1, an enzyme in the KynA biosynthetic pathway (Cheong and Sun, 2018), did not alter the GPR35 contribution to neutrophil recruitment (Figure S2J). In a second model, we observed a GPR35 KO neutrophil recruitment defect into LNs that were inflamed following s.c.

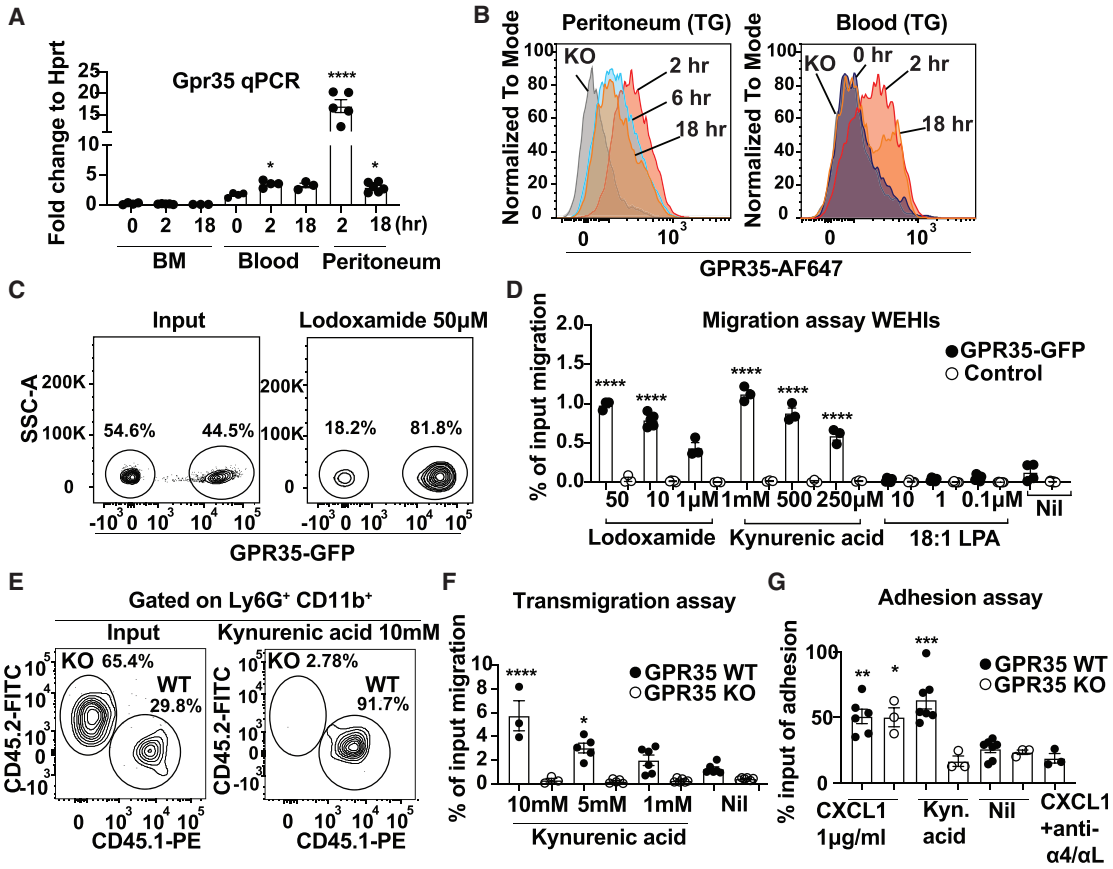

Figure 1. GPR35 is a neutrophil chemotactic receptor

(A) qPCR for expression of Gpr35 (relative to Hprt) in Ly6G$^+$ Ly6C$^+$ CD11b$^+$ CXCR2$^+$ neutrophils sorted from BM, blood, or peritoneum at indicated time points after TG injection (n = 3–6).

(B) Intracellular flow cytometry for GPR35 in Ly6G$^+$ CD11b$^+$ Ly6C$^+$ neutrophils from peritoneum (left) or blood (right) at indicated time points after TG.

(C) Representative flow cytometry plots of GPR35-GFP and control WEHI-231 cells migrating to 50 μM Lodoxamide compared with input.

(D) Quantification of transwell migration assays of GPR35-GFP (black) or control (white) WEHI-231 cells to Lodoxamide, KynA or 18:1 LPA at the indicated concentrations (n = 3–6).

(E and F) Representative flow cytometry plots (E) and quantification (F) of transmigration assay with GPR35 WT (CD45.1) or KO (CD45.2) peritoneal neutrophils 2 h after TG, migrating to KynA at indicated concentrations (n = 3–6).

(G) Quantification of adhesion assays performed with GPR35 WT or KO peritoneal neutrophils 2 h after TG. Data are pooled from at least two independent experiments. Statistics in (A, D, F, and G) show comparison of all samples to BM 0 h (A) or Nil (D, F and G). *p < 0.05, **p < 0.005, ***p < 0.001, ****p < 0.0001. Data are presented as mean ± SEM. See also Figure S1.

injection with *Listeria* (Figures 2D and S2K–S2N). A similar defect was observed in recruitment to the site of *Listeria* injection in the skin (Figures 2E and S2O). BM neutrophil frequency and the surface phenotype of BM and peritoneal neutrophils were unchanged in GPR35-deficient compared with WT (Figures S3A–S3C) and migration of BM neutrophils in response to other chemoattractants was unaltered (Figure S3D).

Listeria is a cause of peritonitis in humans (Eisa et al., 2018; Poulsen et al., 2018; Tablang, 2008). Following intraperitoneal infection with *Listeria*, the recruited neutrophils were GPR35^{hi} (Figure 2F), and there was 2-fold less neutrophil recruitment in GPR35-deficient mice (Figure 2G). In accord with the defect in neutrophil recruitment, GPR35-deficient mice were less efficient at clearing *Listeria* from the peritoneum (Figure 2H). *E. coli* is another cause of human peritonitis (Facciorusso et al., 2019). GPR35 KO neutrophils were less efficiently recruited to the *E. coli* infected peritoneum (Figure 2I), and GPR35-deficient mice were less able to clear the bacteria (Figures 2J and 2K). Ablation of neutrophils prior to the bacterial infections caused a loss of the GPR35 KO phenotype, consistent with GPR35 being required in neutrophils for bacterial clearance (Figures 2H and 2K). Using mixed BM chimeric mice in which the only lineage fully deficient in GPR35 was neutrophils, we again observed a defect in clearance of bacteria from the peritoneum (Figure 2L).

In the peritoneal inflammation experiments, all the neutrophils measured in the peritoneal lavage fluid are extravascular. Many neutrophils enter the peritoneum via the omentum, a sheet-like tissue composed of mesothelial cells and containing adipocytes, endothelial cells, and aggregates of macrophages and lymphocytes in so-called "milky spots" (Buscher et al., 2016;

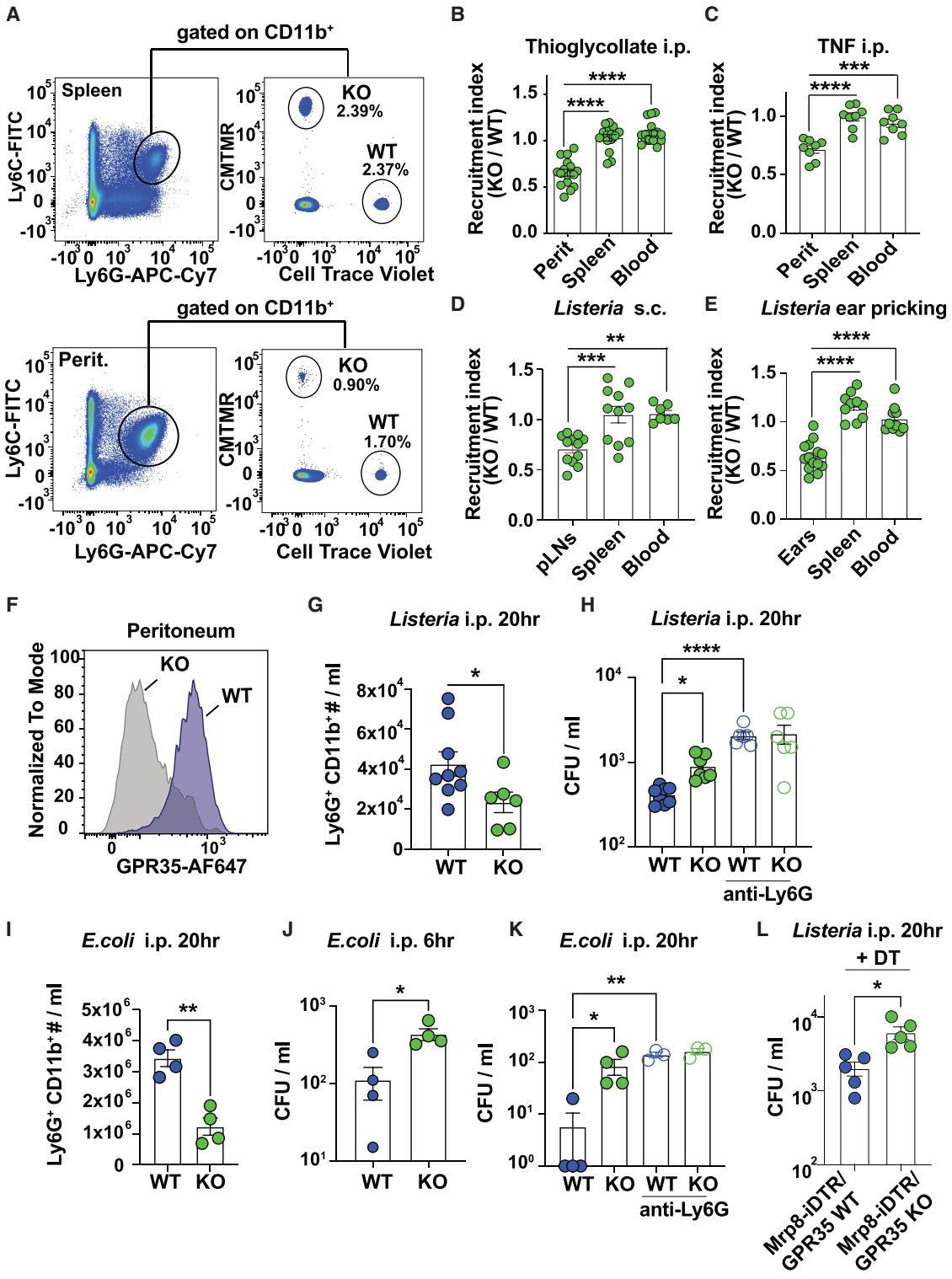

Figure 2. GPR35 sustains neutrophil recruitment to inflamed tissues

(A) Representative flow cytometry plots of spleen (top) and peritoneum (bottom) from mice injected with a 50:50 mix of GPR35 WT (cell trace violet) and GPR35 KO (CMTMR) BM neutrophils, 18 h after i.p. TG treatment.

(B) Graphs showing neutrophil recruitment index (% KO/% WT) of mice exemplified in (A) (n = 15–16).

(legend continued on next page)

Jackson-Jones et al., 2020). Flow cytometric analysis of intravascularly labeled cells showed that a significantly greater fraction of the GPR35-deficient neutrophils in the omentum were blood exposed 2 h after transfer (Figures 3A and 3B). Taken together, the findings suggested that the reduced accumulation of extravascular neutrophils in the peritoneum reflected reduced migration from vessels into omental tissue and not reduced attachment to the endothelium.

Intravital 2-photon microscopy was employed to gain dynamic information regarding the post-attachment recruitment step that was affected by GPR35-deficiency. To permit visualization of WT and GPR35-deficient neutrophils in the same animals, BM from Mrp8-Cre × mTmG mice in which neutrophils express GFP was mixed with BM from GPR35-deficient mice and used to reconstitute irradiated WT recipients. To permit visualization of all neutrophils, mice were pretreated with phycoerythrin (PE)-conjugated Ly6G antibody. Imaging of the omentum in these BM chimeras showed that GPR35-deficient neutrophils were less efficient at moving from the vessel lumen into the parenchyma (Figures 3C–3F; videos S1 and S2). Similar observations were made with transferred fluorescently labeled neutrophils (video S3), although the low frequencies of transferred cells in each imaging volume made this approach less quantitative. Figure 3G shows a zoomed-in view of a transmigration event. GPR35 KO neutrophil track speed within vessels was increased (Figure S4A), whereas no differences were observed in total cell track speed that included many cells in the parenchyma (Figure S4B). Microscopy on the skin of WT:GPR35 KO mixed BM chimeras showed a similar dependence on GPR35 for neutrophil movement from blood vessel into tissue (Figures S4C–S4F; video S4), and the cells showed a trend for increased speed (Figure S4G); in this tissue, total GPR35-deficient cells also had a slightly increased track speed (Figure S4H). These data suggest that GPR35 contributes, along with other chemoattractant factors, to promoting transendothelial migration of activated neutrophils and that this activity involves a reduction in speed perhaps due to GPR35-promoting increased adhesion of crawling cells.

5-HIAA is an endogenous GPR35 ligand

Using an *in vitro* migration-based bioassay, we screened tissue extracts for GPR35 ligand activity and found activity in serum (Figure 4A). Serum is made up of plasma and the contents of activated platelets. Serum had stronger GPR35 ligand activity than plasma, consistent with platelets functioning as a source of ligand (Figure 4A). Indeed, activated platelet supernatant promoted attraction of GPR35$^+$ cells (Figures 4B and 4C). Platelet supernatant was also able to cause GPR35 internalization (Figure S5A). Platelets have not been identified as a source of KynA and have minimal expression of KynA synthetic enzymes (Manne et al., 2020; Wirthgen et al., 2018), but they are an important reservoir of gut-derived serotonin (5-Hydroxytryptamine), another tryptophan metabolite (Berger et al., 2009). Serotonin was inactive in recruiting GPR35$^+$ cells (Figure S5B) in accord with earlier data (Wang et al., 2006). Platelets express monoamine oxidase-B (MAO-B), and they metabolize serotonin into 5-HIAA, and their dense granules contain 5-HIAA, as well as serotonin (Berger et al., 2009; Pletscher, 1968; Shad and Saeed, 2007). Strikingly, 5-HIAA was a potent chemoattractant of mouse and human GPR35$^+$ cells (Figures 4D, 4E, and S5C), and it could promote GPR35$^+$ cell adhesion to endothelial monolayers (Figure S5D). 5-HIAA was also effective in promoting activated neutrophil migration (Figure 4F) and their transmigration across an endothelial monolayer in a GPR35-dependent manner (Figure S5E). Mixing CXCL1 and 5-HIAA had an additive effect in promoting activated neutrophil adhesion and transmigration (Figures S5F and S5G). Confirming that 5-HIAA was acting as a GPR35-ligand, it caused internalization of the murine and human receptor from the cell surface in a dose-dependent manner, whereas it did not internalize a control GPCR (Figures 4G–4I and S5H).

GPR35 function in neutrophil recruitment involves platelets

Since platelet-derived 5-HIAA could promote migration of GPR35$^+$ cells *in vitro*, we explored the contribution of platelets to GPR35-mediated neutrophil recruitment *in vivo*. By real-time imaging of PF4-Cre$^+$ mTmG reporter mice that harbor GFP$^+$ platelets, a dense accumulation of platelets was observed on the inflamed endothelium in the omentum (Figure 5A), as well as in LNs and skin (Figure S6A). Neutrophils were observed attached to platelet-coated endothelial surfaces and often crossed the endothelium in these regions (Figure 5A; videos S5 and S6). GPR35-deficient neutrophils showed reduced association with platelets and most notably, reduced transmigration in platelet-rich regions (Figures 5A and S6B; videos S5 and S6). Quantitation showed that GPR35-deficient cells had reduced platelet contact and reduced total time in contact and a greater distance of transmigrating cells from platelets (Figures 5B, 5C, S6C, and S6D). Neutrophil interaction with platelets can lead to neutrophils acquiring platelet membrane markers (Page and Pitchford, 2013). Flow cytometric analysis showed reduced acquisition of the platelet marker CD41 (Itga2b/GPIIb) by GPR35-deficient neutrophils in peritoneally inflamed mice, consistent with the reduced intravascular neutrophil-platelet contact (Figures 5D and S6E).

Neutrophil transfers into platelet-deficient mice showed that GPR35 was less able to augment neutrophil recruitment to

(C–E) Quantification of transferred neutrophil recruitment index in mice injected with either i.p. TNF (2 h, n = 8) (C), s.c. *Listeria* (20 h, n = 10) (D), or pricked with *Listeria*-contaminated needle (2 h; ears, n = 11; spleen, blood, n = 7) (E).
(F) Intracellular flow cytometry for GPR35 in Ly6G$^+$ CD11b$^+$ Ly6C$^+$ neutrophils from peritoneum of WT or GPR35 KO mice 20 h after *Listeria* injection.
(G) Quantification of endogenous neutrophil numbers 20 h after peritoneal *Listeria* infection (WT, n = 9; GPR35 KO, n = 6).
(H) Quantification of *Listeria* peritoneal CFUs (WT, n = 8; KO, n = 7) 20 h after i.p. infection in mice treated or not with Ly6G depleting antibody.
(I) Quantification of endogenous neutrophil numbers 20 h after peritoneal *E. coli* infection (n = 4).
(J and K) Quantification of *E. coli* peritoneal CFUs 6 h (J, n = 4) and 20 h (K, n = 4) after i.p. infection in mice treated or not with Ly6G depleting antibody.
(L) Quantification of *Listeria* peritoneal CFUs (n = 5) in Mrp8-Cre × iDTR/GPR35 WT or KO mixed chimeras treated with DT, 20 h after *Listeria* infection. Data are pooled from at least two independent experiments. *p < 0.05, **p < 0.005, ***p < 0.001, **** p < 0.0001. Data are presented as mean ± SEM. See also Figures S2 and S3.

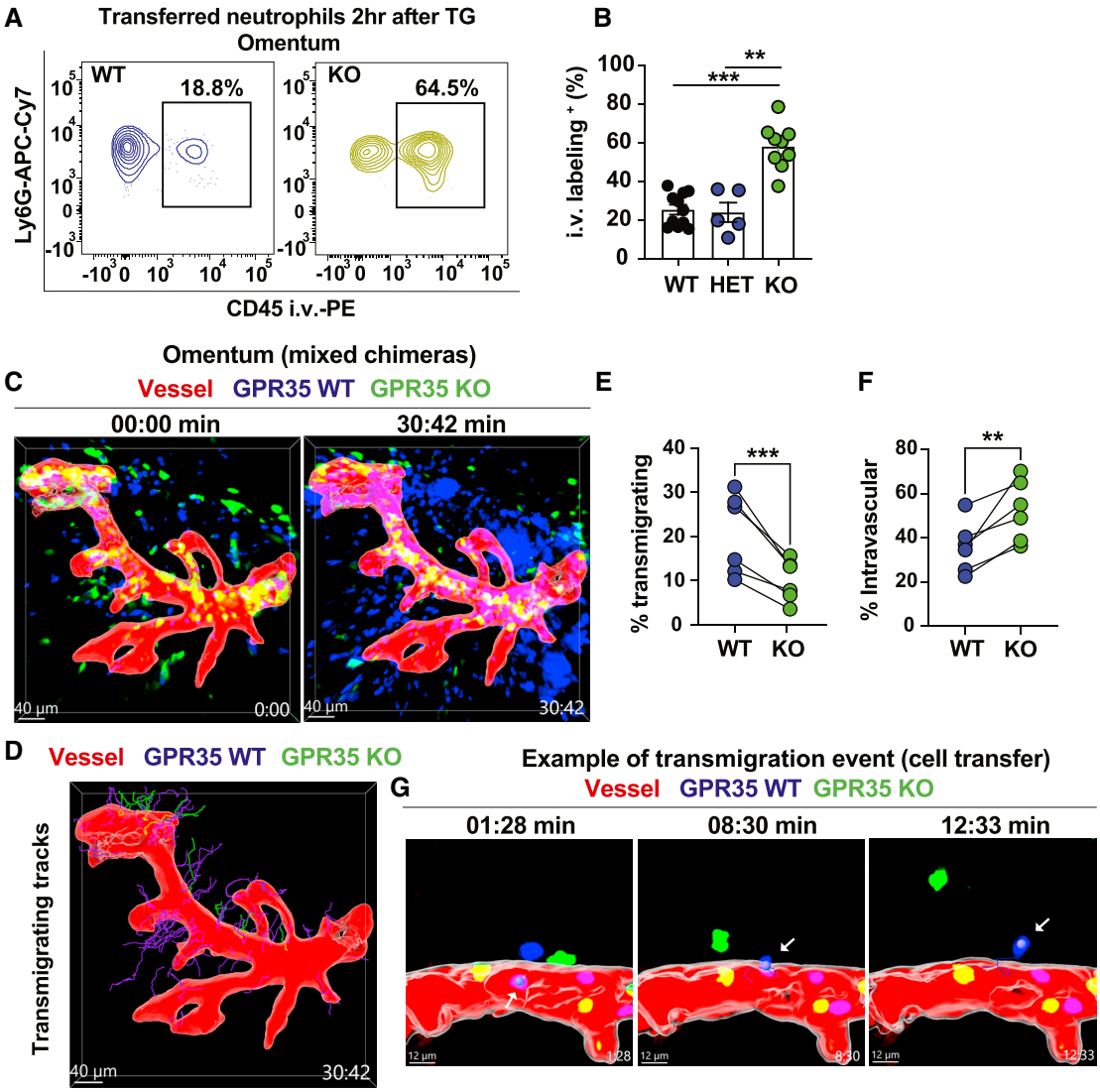

Figure 3. GPR35 supports neutrophil *in vivo* transendothelial migration

(A) Representative flow cytometry plots showing % of CD45-PE^{+} intravascular WT (left) or GPR35 KO (right) transferred neutrophils in the omentum 2 h after i.p. TG.

(B) Quantification of data shown in (A) (WT, n = 11; HET, n = 5; KO, n = 9). Data are pooled from three independent experiments.

(C) Multiphoton intravital micrographs of Mrp8-Cre^{+} mTmG (blue) and GPR35 KO (green) neutrophils in the omentum of mixed BM chimeric mice injected with labeled dextran to identify vessels (red) and with Ly6G-PE to label neutrophils, 2 h post TG. Time shown in min:s, see also Video S1.

(D) Intravital micrograph showing transmigrating (WT blue, KO green) tracks from Video S1. Image is representative of at least three independent intravital movies.

(E and F) Quantification of transmigrating (E) or intravascular (F) track % of WT or KO neutrophils in the omentum of mice of the type in (C), 2 h after TG (n = 6).

(G) Intravital micrographs of CTV-WT (blue) or CFSE-KO (green) transferred neutrophils in the omentum of mice injected with dextran-rhodamine and anti-CD31 PE to identify vessels (red), 2 h post TG (Video S3). Time shown in min:s. Arrow highlights transmigrating cell. Data are representative of 4-cell-transfer movies.

**p < 0.005, ***p < 0.001. Data are presented as mean ± SEM. See also Figure S4.

inflamed skin since wild-type and GPR35 KO cells were recruited more similarly (Figure 5E). Moreover, WT, but not KO neutrophils, showed higher labeling by intravascular antibody in skin-inflamed platelet-deficient mice, indicating less efficient movement from blood vessels into the tissue parenchyma (Figure 5F). Enumeration of the recruited transferred cells confirmed the platelet dependence of GPR35 function and showed that platelet deficiency had a further effect on neutrophil recruitment (Figure S6F), consistent with multiple platelet-derived factors being involved in recruitment. A similar platelet dependence of GPR35 function was observed in *Listeria*-inflamed LNs (Figure 5G). Homing to peritoneum could not be readily studied in platelet-deficient mice due to the strong inflammation frequently causing blood leakage into the peritoneum in the absence of platelets. Taken together, these data strongly implicate platelets, likely acting as a source of 5-HIAA, in GPR35-mediated neutrophil recruitment.

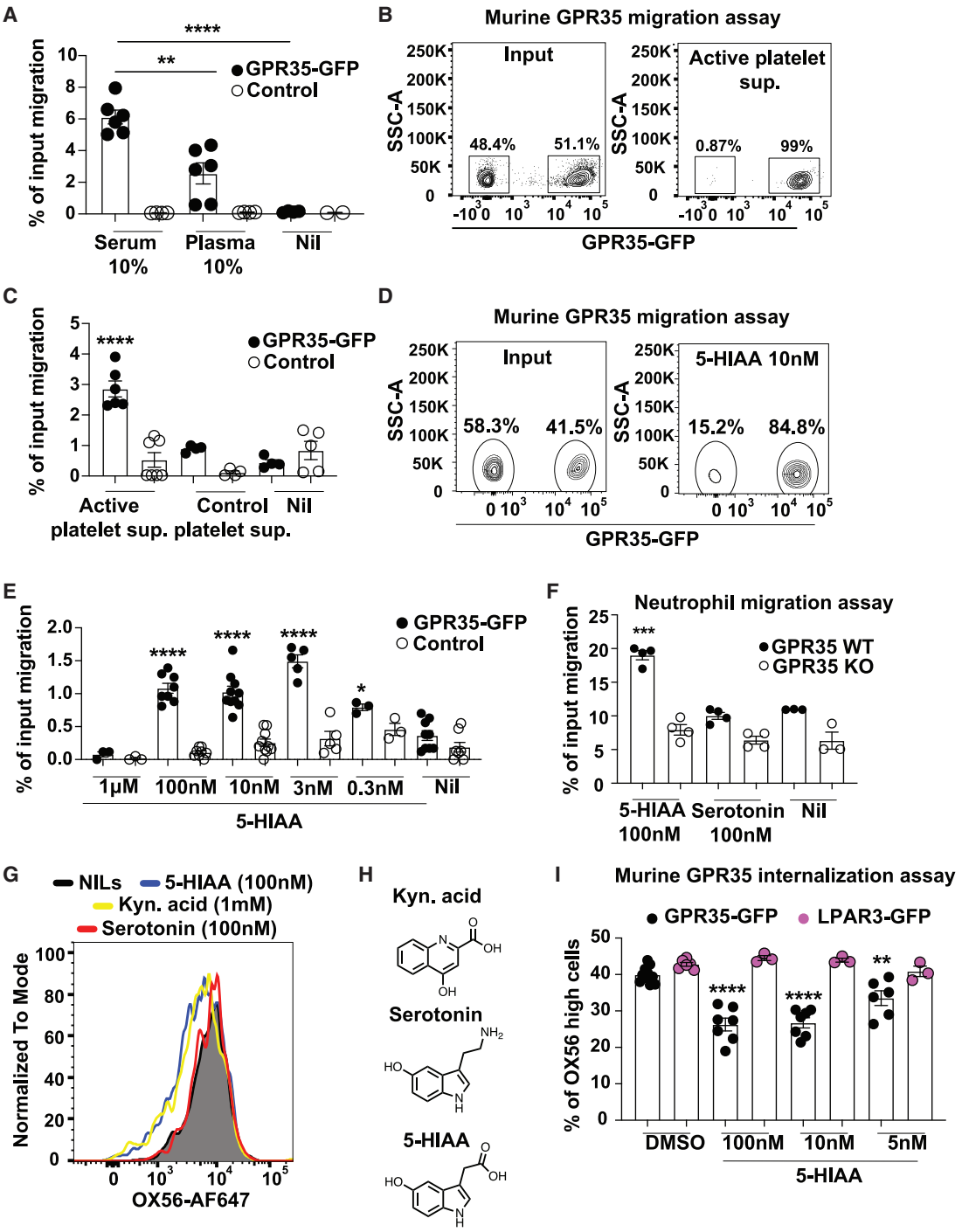

Figure 4. Platelet-derived 5-HIAA is a potent GPR35 ligand

(A) Quantification of transwell migration assay of GPR35-GFP or control WEHI-231 cells to 10% mouse serum or plasma (GPR35-GFP: n = 6; Nil, n = 4; control: n = 5; Nil, n = 2). Data are pooled from two independent experiments.

(B and C) Representative flow cytometry plots (B) and quantification (C) of GPR35-GFP (black) or control (white) WEHI-231 cells migrating to activated or resting (control) platelet culture supernatants (n = 4–7). Data are pooled from three independent experiments.

(D and E) Representative flow cytometry plots (D) and quantification (E) of GPR35-GFP and control WEHI-231 cell transwell migration to 5-HIAA at indicated concentrations (n = 3–10).

(F) Quantification of WT or GPR35 KO peritoneal neutrophil (2 h after TG) transwell migration to 100 nM 5-HIAA or serotonin (Nil, n = 3; all others, n = 4). Data are pooled from four (E) ortwo2 (F) independent experiments.

(legend continued on next page)

Mast cells contribute to GPR35-mediated recruitment of neutrophils

Platelets do not synthesize serotonin but acquire it from intestinal epithelial cells (Berger et al., 2009). The one peripheral cell type beyond intestinal epithelium that highly expresses Tph1 and synthesizes serotonin is the mast cell (Herr et al., 2017; Nowak et al., 2012; Yabut et al., 2020). Mast cells also express MAO (Immgen.org), and a few studies have suggested that they can be a source of 5-HIAA (Freitag et al., 1995; Gershon et al., 1975; Lehtosalo et al., 1984; Sjoerdsma et al., 1957). We found that activation of peritoneal mast cells with lipopolysaccharide (LPS) led to generation of extracellular 5-HIAA and the mast cell supernatant was active in attracting GPR35^{+} cells (Figures 6A and 6B). The P815 mastocytoma cell line constitutively released 5-HIAA (Figure 6C). Treatment with anti-5-HIAA blocked GPR35-dependent cell migration to mast cell supernatants and to serum (Figures 6D and 6E). We then observed that mast cell-deficient mice supported reduced GPR35-dependent recruitment of neutrophils to *Listeria*-inflamed skin (Figure 6F). Intravascular labeling showed that the GPR35-dependent exit of cells from the skin vascular compartment required mast cells (Figure 6G). *Listeria* inoculation in the skin caused rapid mast cell activation, measured by CD63 upregulation (Figure 6H). To examine the sufficiency of mast cell-derived 5-HIAA to promote neutrophil recruitment, we performed experiments in platelet-depleted mice. *Listeria* induced less mast cell activation in platelet-depleted mice (Figure 6H), in accord with the evidence that platelets trigger activation of perivascular mast cells (Karhausen et al., 2020). Treatment of *Listeria* inoculated platelet-depleted mice with the mast cell-triggering compound 48/80 (Freitag et al., 1995) was able to restore mast cell activation (Figure 6H), and this treatment increased the GPR35-dependence of neutrophil recruitment (Figure 6I). Additionally, injection of 5-HIAA into the skin of mast cell-deficient mice at the same time as *Listeria* inoculation promoted GPR35-dependent neutrophil recruitment, determined both by the efficiency of recruitment of transferred cells (Figure 6J) and by enumerating the recruitment of endogenous neutrophils (Figure 6K). These data are consistent with the possibility of mast cell-derived 5-HIAA cooperating with platelet-derived 5-HIAA during neutrophil recruitment.

5-HIAA is required for GPR35-mediated neutrophil recruitment

Fluoxetine (Prozac™) is a serotonin uptake inhibitor and chronic fluoxetine treatment is well established to prevent serotonin accumulation (and 5-HIAA generation) selectively in platelets due to their lacking Tph1 and acquiring intestinal serotonin from circulation (Berger et al., 2009). Three week treatment of mice with fluoxetine reduced the recruitment of transferred WT neutrophils to the inflamed skin but did not cause further reduction in recruitment of GPR35 KO cells when assessed as a percent of total cells recruited (Figures 7A and 7B). This was also seen when the data were plotted as a recruitment index (Figure 7C). Treatment with phenelzine to inhibit MAO and block serotonin conversion to 5-HIAA in both platelets and mast cells (Bortolato et al., 2008) had a similar effect in reducing the percent of WT but not causing significant further reduction in the percent of GPR35-deficient neutrophil recruitment (Figures 7A–7C). Plotting the numbers of WT neutrophils recruited showed strong reductions after both fluoxetine and phenelzine treatment (Figure S7A). Significantly less GPR35 KO cells were recruited under control treatment conditions, but there was a trend toward a further reduction after fluoxetine treatment and a significant further reduction after phenelzine treatment (Figure S7A). GPR35-independent effects of drug treatment are consistent with the contributions of platelet-derived serotonin to neutrophil recruitment (Berger et al., 2009; Duerschmied et al., 2013; Kubes and Gaboury, 1996). Intravascular labeling in inflamed mice showed that the intravascular accumulation bias of GPR35-deficient skin neutrophils observed in control recipients was lost in phenelzine-treated recipients (Figures 7D and 7E). Fluoxetine and phenelzine treatment also reduced the skin homing efficiency of endogenous neutrophils, and there was increased intravascular labeling of neutrophils in the inflamed skin (Figures 7F and 7G). Importantly, supernatant from activated platelets purified from fluoxetine or phenelzine-treated mice was less effective in promoting GPR35-dependent chemotaxis (Figure 7H) and contained significantly reduced amounts of 5-HIAA (Figure 7I).

As an MAO inhibitor, phenelzine would be expected to reduce 5-HIAA production by both platelets and mast cells. We, therefore, treated platelet-deficient mice with phenelzine in an attempt to measure the impact of blocking mast cell generation of 5-HIAA. Although *Listeria* was less effective in promoting mast cell activation and GPR35-dependent neutrophil recruitment in the absence of platelets, some mast cell activation did occur (Figure 6F), and there was a trend for a GPR35 contribution to the recruitment in the absence of platelets (Figures 5E and 6I). In accord with the detection of some platelet independent GPR35 recruitment activity, phenelzine treatment of platelet-deficient mice led to a reduction in *Listeria*-induced neutrophil recruitment to the skin (Figure 7J).

In another approach, mice were treated with a large intravenous dose of 5-HIAA to disrupt endogenous 5-HIAA gradients. Two hours after the treatment, the plasma 5-HIAA concentration was in the near-micromolar range (Figure S7B), well above the low nanomolar concentration found in normal mouse and human plasma (Figure S7B) (Callebert et al., 2006; Pietraszek et al., 1991; Sano et al., 1993; Tanaka et al., 2021; Tohmola et al., 2014). This treatment caused reduced recruitment of transferred WT but not GPR35-deficient neutrophils to the inflamed skin and peritoneum (Figures S7C and S7D). The treatment also reduced homing of endogenous WT neutrophils to the inflamed peritoneum (Figure S7E) and skin (Figure S7F). In contrast, treatment

(G) Representative flow cytometry histograms of OX56-GPR35 levels in transduced WEHI-231 cells after incubation with 1 mM KynA (yellow), 50 μM Lodoxamide (red), 100 nM 5-HIAA (blue), or Nil (black). Image is representative of at least four independent experiments.
(H) Diagrams of KynA, serotonin, and 5-HIAA molecular structures.
(I) Quantification of OX56 levels in murine OX56-GPR35 and OX56-LPAR3 WEHI-231 cells incubated with 5-HIAA at indicated concentrations (n = 3–11). Data are pooled from four independent experiments. *p < 0.05, **p < 0.005, ***p < 0.001, ****p < 0.0001. Data are presented as mean ± SEM. See also Figure S5.

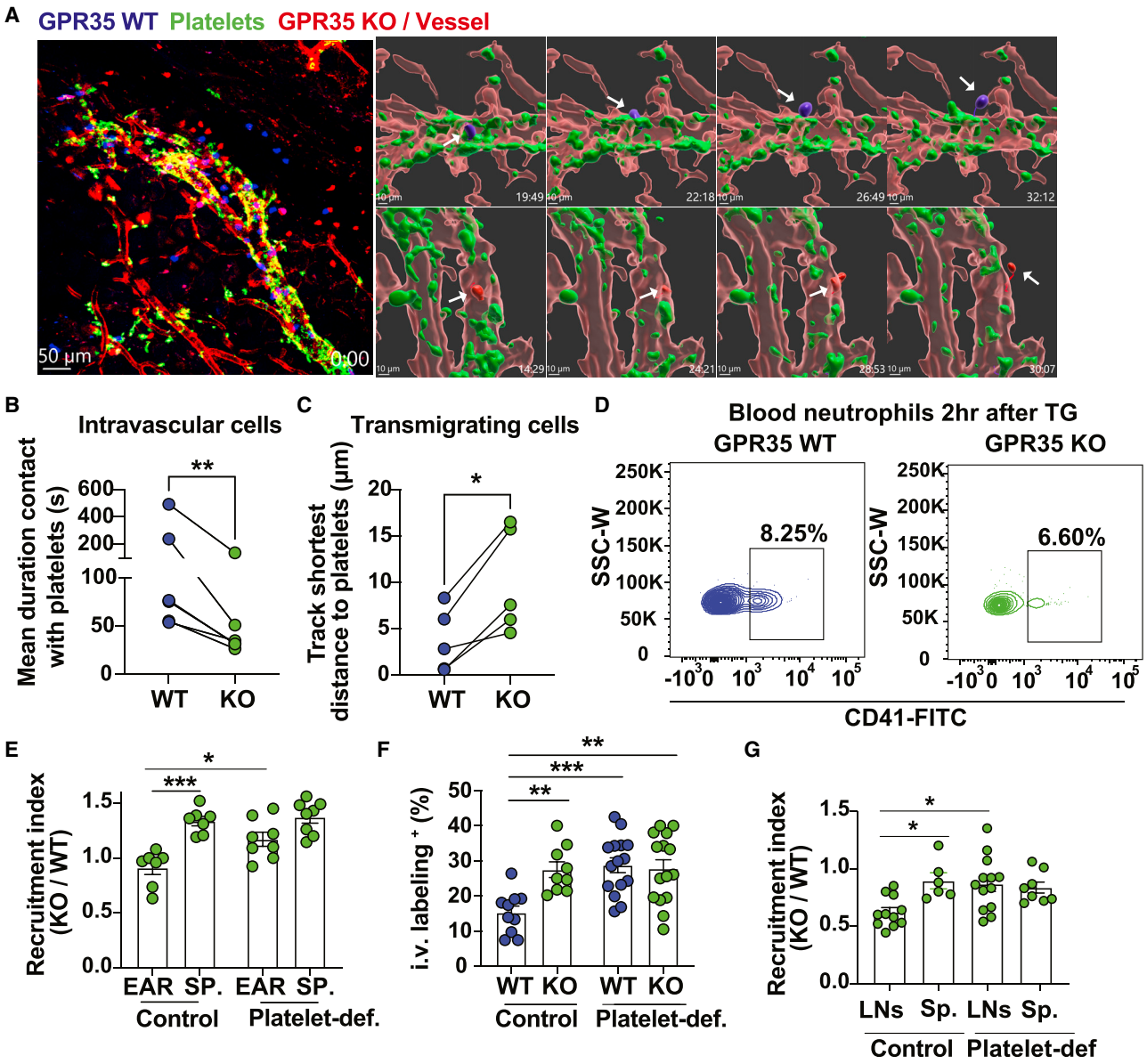

Figure 5. Activated platelets promote GPR35-dependent neutrophil transmigration

(A) Multiphoton intravital micrographs of CTV-WT (blue) or CMTMR-GPR35 KO (red) neutrophils in the omentum of Pf4-Cre × mTmG (platelets GFP$^+$, green) recipients 2 h after TG (see also Video S5). Vessels identified based on tdTom distribution (red). Images are representative of three independent intravital movies. (Left) Composite image at time 0. (Right) Time series showing example WT (upper) and KO (lower) cells transmigrating (arrow). Endothelium shown as an iso-surface based on tdTom fluorescence. Time stamp shows min:s.

(B and C) Quantification of mean contact time with platelets (B) (n = 6) and transmigrating track shortest distances from platelets (C) (n = 6) of images of the type in (A) and Video S5. Each dot represents individual movies.

(D) Representative flow cytometry plots showing % of CD41$^+$ WT (left) or KO (right) transferred neutrophils in blood 2 h after TG.

(E and F) Quantification of (E) neutrophil recruitment index in WT (n = 7) or platelet-deficient (n = 8) and (F) intravascular neutrophil % in WT (left; WT, n = 10; KO, n = 9) or platelet-deficient (right; n = 15) mice 2 h after *Listeria* skin pricking.

(G) Quantification of neutrophil recruitment index in LNs and spleen of WT or platelet-deficient mice (n = 8–13). Data are pooled from at least two independent experiments. *p < 0.05, **p < 0.005, ***p < 0.001. Data are presented as mean ± SEM. See also Figure S6.

with an equivalent dose of KynA was without effect (Figure S7G). The 5-HIAA treatment did not alter the frequency of neutrophils, including marginated cells, in lungs, spleen, or BM (Figures S7H and S7I).

Next, we examined SERT KO mice that lack 5-HIAA in platelets (Bengel et al., 1998; Berger et al., 2009). In accordance with the fluoxetine treatment results, there was reduced GPR35-dependent homing of transferred neutrophils to the

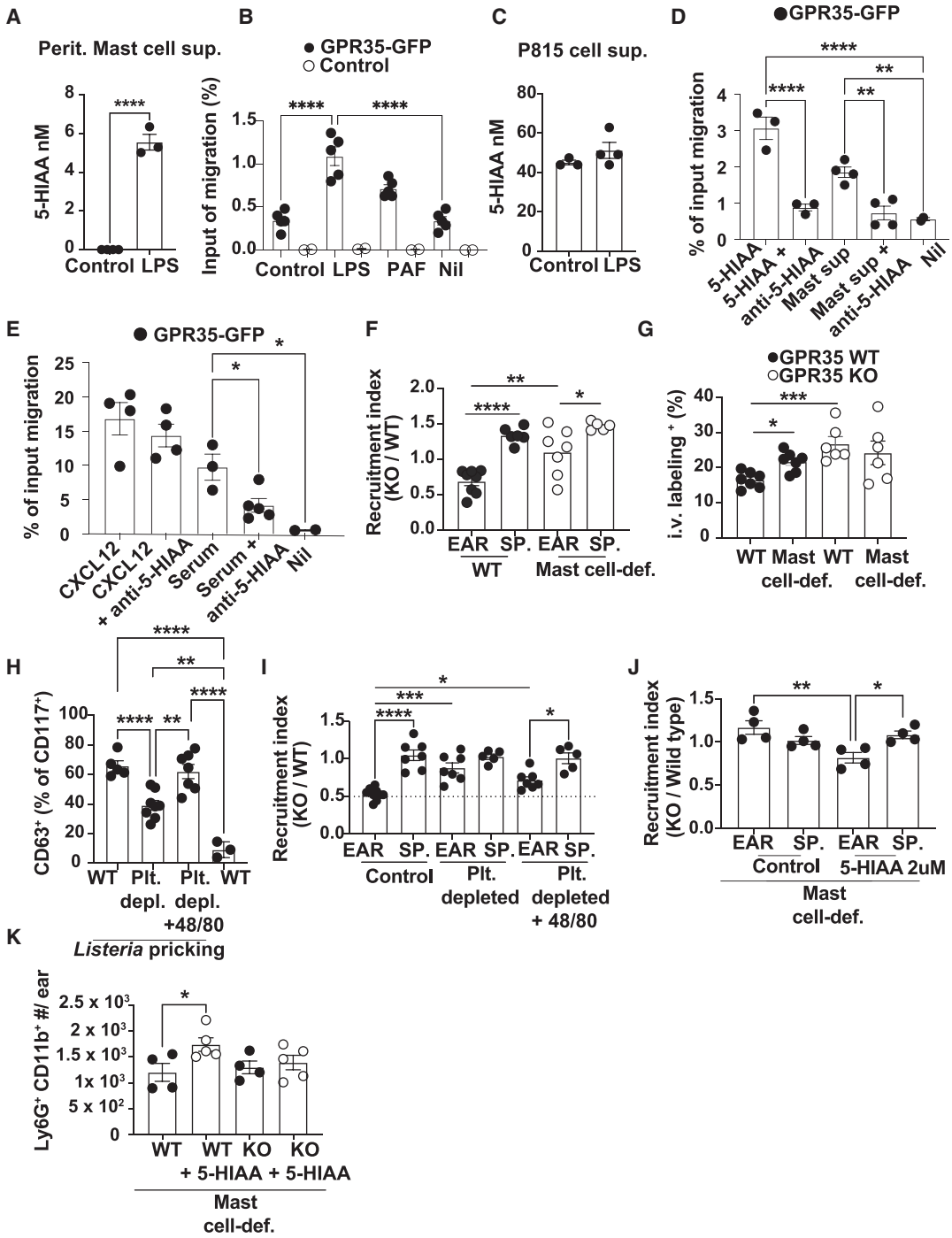

Figure 6. Activated mast cells are sources of 5-HIAA and collaborate with platelets to sustain GPR35-dependent neutrophil recruitment

(A) Graph showing ELISA quantification of 5-HIAA in control (n = 4) or LPS-treated (n = 3) peritoneal mast cell supernatants. Single dots represent biological replicates. Unpaired t test was applied: ****p < 0.0001.

(B) Quantification of GPR35-GFP WEHI-231 cell migration to control or LPS-treated peritoneal mast cell supernatants (n = 5).

(C) Graph showing ELISA quantification of 5-HIAA in control (n = 3) or LPS-treated (n = 4) P815 mast cell line supernatants.

(D and E) Quantification of GPR35-GFP WEHI-231 cell migration to (D) 5-HIAA (5 nM), mast cell supernatants (50%), (E) CXCL12 (100 ng/mL), or serum (5%) with the addition of anti-5-HIAA (2 μg/mL) as indicated (n = 2–5).

(F and G) Transferred neutrophil recruitment index (n = 5–8) (F) and i.v. labeling (n = 6–7) (G) in WT or mast cell-deficient mice 2 h after *Listeria* pricking.

(legend continued on next page)

inflamed skin of SERT KO mice (Figures 7K and S8A) and reduced recruitment of endogenous neutrophils (Figure S8B). To confirm that this reflected a role for SERT in platelets, we examined mixed BM chimeras where full SERT deficiency was restricted to platelets. As in SERT KO mice, there was reduced GPR35-dependent neutrophil recruitment to the inflamed ear skin (Figures S8C–S8E).

To genetically disable 5-HIAA production in mast cells, we reconstituted lethally irradiated WT mice with BM from Tph1 KO mice (Côté et al., 2003). Such chimeric mice retain Tph1 expression in gut epithelium, the source of platelet 5-HIAA (Berger et al., 2009). Mast cells from the Tph1 KO BM chimeras were confirmed to have significantly reduced ability to produce 5-HIAA (Figure S8F). Tph1 KO BM chimeras showed reduced GPR35-dependent recruitment of transferred neutrophils to *Listeria* inoculated ear skin (Figures 7L and S8G) and reduced recruitment of endogenous neutrophils (S8H). Taken together, these data indicate that 5-HIAA is an *in vivo* ligand of GPR35, and they provide the evidence that both platelets and mast cells contribute to 5-HIAA production at sites of inflammation.

DISCUSSION

This study reveals that the major serotonin metabolite, 5-HIAA, acts as a physiological ligand for GPR35 and thereby promotes neutrophil recruitment to the sites of inflammation and bacterial clearance. Our data suggest that platelet- and mast cell-derived 5-HIAA cooperate non-redundantly in neutrophil recruitment, working with other mediators produced by these cells. In the simplest model, we propose that platelet-derived 5-HIAA promotes adhesion of crawling neutrophils in association with platelet clusters and that mast cell-derived 5-HIAA provides directional signals during transmigration. The ability of platelets and mast cells to cross-activate each other may amplify these events (Karhausen et al., 2020; Schwartz, 1987). Our study does not fully exclude the roles for other cell types as sources of neutrophil-recruiting 5-HIAA. GPR35 and 5-HIAA are likely to contribute to the recruitment of additional GPR35$^+$ blood cells, such as monocytes, to sites of inflammation, and they may also guide myeloid cell migration within tissues (Barth et al., 2009; Kaya et al., 2020; Pagano et al., 2021; Quon et al., 2020; Slaba et al., 2015).

Serotonin was discovered over 70 years ago, and it is known to have wide ranging influences on animal physiology, but 5-HIAA has been considered to merely be its waste metabolite (Berger et al., 2009; Bortolato et al., 2010). Our findings add to the nascent evidence that 5-HIAA is itself an intercellular signaling molecule, with one study suggesting that it acts as a ligand for the aryl hydrocarbon receptor (Rosser et al., 2020) and work in *C. elegans* suggesting that it modulates RAS/MAPK signaling (Schmid et al., 2015). Serotonin acts on the endothelium to promote vascular leakiness and leukocyte rolling interactions, with the latter involving mobilization of endothelial cell adhesion molecules (Askenase et al., 1980; Berger et al., 2009; Duerschmied et al., 2013; Kubes and Gaboury, 1996). We suggest that serotonin and 5-HIAA may often cooperate during the neutrophil recruitment process. Our findings prompt the need to consider how widely used serotonin (and thus 5-HIAA) modulating drugs (Berger et al., 2009; Bortolato et al., 2008) or neuroendocrine tumors that lead to markedly elevated plasma 5-HIAA (Lindström et al., 2018) influence GPR35-mediated processes. Depending on the inflammatory condition, reduced neutrophil recruitment in mice treated chronically with fluoxetine may reflect reduced rolling-mediated attachment to the less activated endothelium (Duerschmied et al., 2013), as well as reduced GPR35 function. Although serotonin has been suggested to act directly on neutrophils (Herr et al., 2017), there is a lack of genetic evidence that neutrophils functionally express serotonin receptors. We suggest that the putative direct actions of serotonin modulators on neutrophils instead involve reductions in 5-HIAA and thus GPR35 function. The doses of fluoxetine and other selective serotonin reuptake inhibitors (SSRIs) used to treat psychiatric conditions in patients may not be sufficient to fully deplete platelets of serotonin and 5-HIAA. However, evidence exists for increased bacterial infections in some SSRI-treated patients and for the occasional development of skin lesions, conditions consistent with reduced neutrophil function (Herstowska et al., 2014; Jarchum et al., 2012; Rogers et al., 2013).

Our finding of an intraluminal enrichment of GPR35-deficient versus WT neutrophils at sites of inflammation suggests that GPR35 deficiency does not impede attachment to the endothelium. However, our findings do not exclude the possibility, suggested based on *in vitro* data (Barth et al., 2009), that GPR35 contributes to the neutrophil rolling-to-sticking transition under some conditions. Platelets are a source of multiple neutrophil recruitment factors, including platelet activating factor, adhesion molecules, and chemokines (Slaba and Kubes, 2017), and 5-HIAA must act in concert with these factors to promote adhesion of crawling neutrophils in association with platelets and their subsequent transmigration across endothelium. Multiple reports have established that platelets augment neutrophil transendothelial migration into tissue, and although their contribution of P-selectin and integrin ligands are well established (Slaba and Kubes, 2017), how the chemoattractive mediators augment the transendothelial migration step remains less understood. As with other platelet-derived chemoattractants, it is unclear whether platelet 5-HIAA is only acting intralumenally, or whether the continual loss of luminal molecules in blood flow allows a transendothelial gradient to be established. In this regard it is notable that platelets were the principal source of serotonin in inflamed tissue of mast cell-deficient mice (Geba et al., 1996). Similar to platelets,

(H) Quantification of CD63$^+$ cells out of total CD117$^+$ mast cells in 2 h *Listeria* pricked skin of control (n = 5), platelet-depleted (n = 8), platelet-depleted + compound 48/80 s.c. (n = 7), or untreated controls (n = 3).
(I) Transferred neutrophil recruitment index (n = 5–7) in control, platelet-depleted, or platelet-depleted and 48/80-treated mice 2 h after *Listeria* pricking. Data pooled from two independent experiments.
(J and K) Transferred neutrophil recruitment index (J) and numbers (K) in mast-cell-deficient mice 2 h after *Listeria* skin pricking and s.c. injection with DMSO (control) or 5-HIAA (n = 4). *p < 0.05, **p < 0.005, ***p < 0.001, ****p < 0.0001. Data are presented as mean ± SEM.

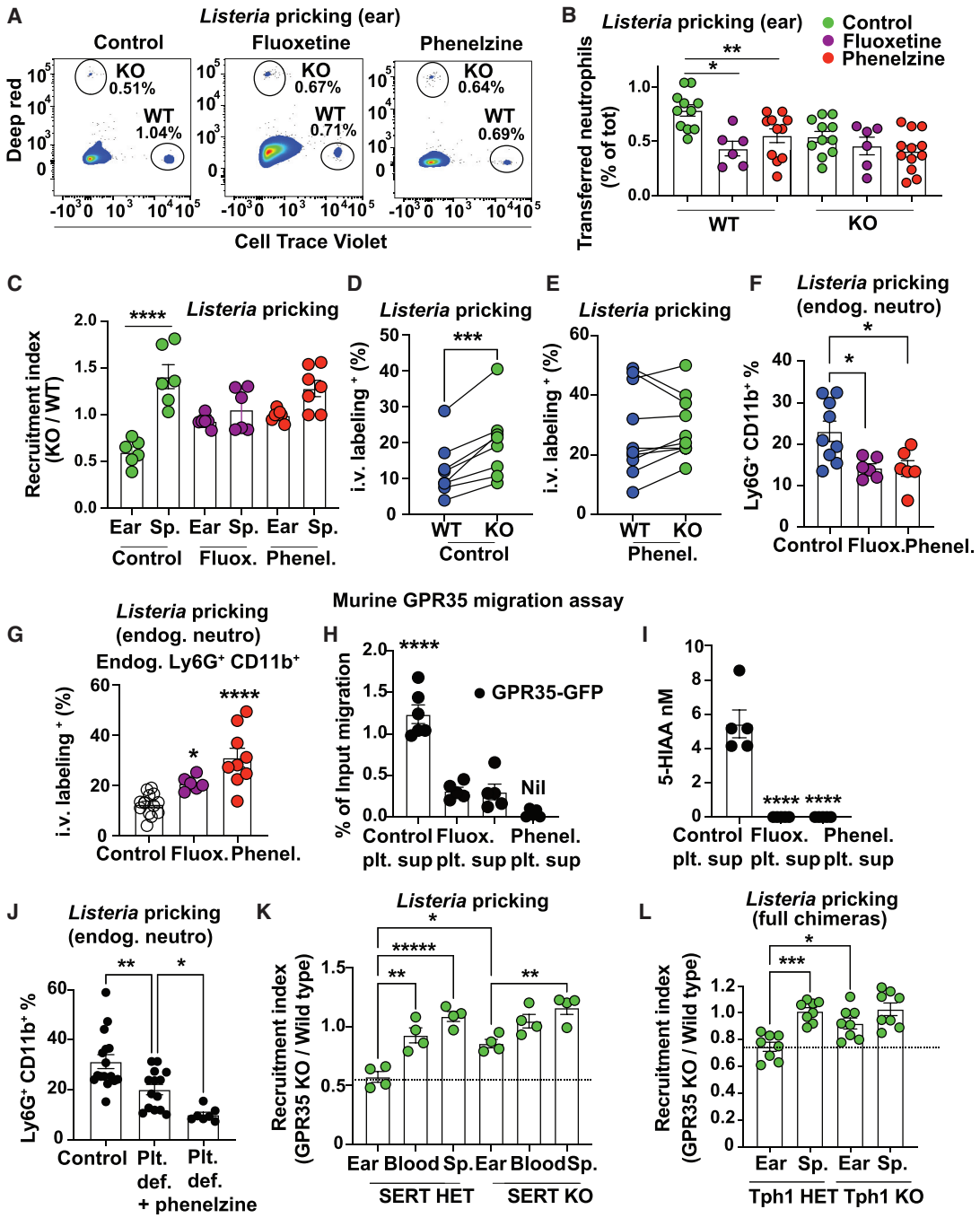

Figure 7. Platelet and mast-cell-derived 5-HIAA promote neutrophil recruitment *in vivo*

(A and B) Representative flow cytometry plots (A) and quantification (B) of % transferred WT or KO neutrophils in ear skin of controls (green) or mice pretreated with fluoxetine (purple) or phenelzine (red), 2 h after *Listeria* skin pricking (n = 6–12).

(C) Graph showing quantification of transferred neutrophil recruitment index in controls or mice pretreated with fluoxetine (purple) or phenelzine (red), 2 h after *Listeria* skin pricking (n = 6–7). Graphs depict bars with mean ± SEM.

(D and E) Quantification of CD45-PE$^+$ intravascular transferred neutrophils in controls (D) and mice treated with phenelzine (E), 2 h after *Listeria* skin pricking (B, n = 8; C, n = 10).

(F and G) Graphs showing quantification of endogenous neutrophil % (F) (WT, n = 9; phenelzine, n = 6; fluoxetine, n = 6) or CD45-PE$^+$ intravascular endogenous neutrophils (G) in mice untreated (n = 14) treated with phenelzine (red) (n = 9) or fluoxetine (purple) (n = 6).

(H) Quantification of GPR35-GFP WEHI-231 cell migration to activated platelet culture supernatants from mice treated with phenelzine or fluoxetine (control platelet sup, n = 6; all others, n = 5).

(legend continued on next page)

mast cells also produce multiple neutrophil chemoattractants (Galli et al., 2020; Wernersson and Pejler, 2014), raising interesting questions about how individual factors have non-redundant roles during the recruitment process. Early cell depletion and drug treatment studies implicated platelet- and mast cell-derived serotonin in cell recruitment events associated with delayed type hypersensitivity (DTH) (Askenase et al., 1980, 1983; Geba et al., 1996). It seems likely that 5-HIAA will also be involved in the DTH response. It will be important to determine the mechanism of 5-HIAA release from mast cells and whether it can be triggered differentially from histamine release, as has been suggested for serotonin (Meixiong et al., 2019; Theoharides et al., 1982). Moreover, whether mast cell Tph1 and MAO continue to act following mast cell activation and thereby allow ongoing 5-HIAA production need investigation.

Although the production of serotonin by murine mast cells is well established, production by human mast cells has been questioned (Sjoerdsma et al., 1957). However, subsequent work showed serotonin in the supernatant of human mast cells in amounts within 5-fold of those produced by mouse mast cells (Enerbäck, 1963; Kushnir-Sukhov et al., 2007; Wernersson and Pejler, 2014). A proteomic study revealed that MAO-B is one of the proteins most enriched in human and mouse mast cells compared with non-mast cells (Plum et al., 2020). Moreover, many patients with mastocytosis had elevated serum serotonin, and patients with urticaria pigmentosa (a condition of elevated skin mast cell activity) had elevated circulating 5-HIAA (Kushnir-Sukhov et al., 2007; Morishima, 1970). Therefore, we contend that, similar to the mouse mast cells, human mast cells contribute to 5-HIAA production and GPR35-mediated cell recruitment at sites of inflammation, but further study of this topic is needed.

GPR35 has been shown to influence intestinal inflammation and colon cancer development, as well as cardiac, vascular, and adipose tissue function (Agudelo et al., 2018; Boleij et al., 2021; Divorty et al., 2018; Farooq et al., 2018; Kaya et al., 2020; Schneditz et al., 2019; Tsukahara et al., 2017). Some of these effects may involve actions in myeloid cells, whereas others may occur through actions in the epithelium or other GPR35-expressing cell types. By identifying 5-HIAA as an *in vivo* ligand for GPR35, our findings will enable advances in understanding actions of GPR35 in physiology and disease. Moreover, this ligand-receptor axis might be targeted by next generation drugs, such as MAO-inhibitors, with reduced blood brain barrier permeability (Gealageas et al., 2018) to modulate GPR35^{+} cell responses in the context of infections, autoinflammatory diseases, sensory neuron responses, and cancer.

Limitations of the study

Although we provide extensive functional evidence that 5-HIAA is a GPR35 ligand, we have not performed binding studies. It will be of interest in the future to determine the 5-HIAA-binding constants using purified GPR35 protein. We also do not exclude the possibility that other metabolites of serotonin or related amines may function as GPR35 ligands under some conditions. Chronic treatment with fluoxetine and genetic deficiency in SERT reduce platelet serotonin content, whereas phenelzine treatment may increase the same, and both conditions can lead to increases in plasma serotonin. By comparing WT- and GPR35-deficient neutrophil migration in the same animals, indirect (systemic) effects of the drug treatments or SERT deficiency are controlled for, but a co-dependence of the observed effects on altered serotonin levels, as well as 5-HIAA levels, cannot be excluded. This is also the case for possible effects of reduced hematopoietic serotonin production in Tph1-deficient BM chimeras.

STAR★METHODS

Detailed methods are provided in the online version of this paper and include the following:

- KEY RESOURCES TABLE
- RESOURCE AVAILABILITY
  - Lead contact
  - Materials availability
  - Data and code availability
- EXPERIMENTAL MODEL AND SUBJECT DETAILS
  - Mice
- METHOD DETAILS
  - Treatments and bone marrow chimeras
  - Flow cytometry and cell sorting
  - Generation of GPR35-expressing WEHI-231 cells
  - Cell lines and treatments
  - Chemicals and reagents
  - Quantitative PCR
  - Transwell migration assay
  - Transendothelial migration assay and adhesion assay
  - Internalization assay
  - Platelet and mast cell purification and activation and 5-HIAA ELISA
  - Intravital imaging
  - Image processing and quantification
- QUANTIFICATION AND STATISTICAL ANALYSIS

SUPPLEMENTAL INFORMATION

Supplemental information can be found online at https://doi.org/10.1016/j.cell.2022.01.010.

ACKNOWLEDGMENTS

We thank Serena Ranucci for technical help with *Listeria* experiments; Jinping An for help with mouse screening, Lihui Duan for help with bioinformatics;

(I) ELISA quantification of 5-HIAA in supernatants of activated platelets from control, phenelzine-treated or fluoxetine-treated mice. Data are representative of two independent experiments.
(J) Quantification of Ly6G^{+} CD11b^{+} endogenous neutrophils in the skin of WT (n = 16), platelet-deficient (n = 14) or platelet-deficient mice treated with phenelzine (n = 7) 2 h after *Listeria* skin pricking. Data are pooled from at least three independent experiments.
(K and L) Transferred neutrophil recruitment index in SERT HET or KO mice (K, n = 4) or Tph1 HET or KO chimeras (L, n = 8) 2 h after *Listeria* skin pricking. Data are pooled from two independent experiments. *p < 0.05, **p < 0.005, ***p < 0.001 ****p < 0.0001. Data are presented as mean ± SEM. See also Figures S7 and S8.

Waliul Khan, Huaquing Wang, and Francine Cote for Tph1-deficient BM; and Eric Dang and Erick Lu for comments on the manuscript. M.D.G. was supported by an EMBO long-term fellowship and is supported by a CRI Irvington Postdoctoral Fellowship. J.G.C. is an investigator of the Howard Hughes Medical Institute. This work was supported in part by NIH grants R01 AI40098, R01 AI45073, R21AI163036, and R01 AI125445.

AUTHOR CONTRIBUTIONS

M.D.G. and J.G.C. conceptualized the study, designed the experiments, analyzed the data, and wrote the manuscript. M.D.G. performed most experiments. H.T. and Y.X. performed *in vitro* assays and provided input on the manuscript. C.V. and M.R.L. purified/activated platelets and provided critical reagents and expertise.

DECLARATION OF INTERESTS

The authors declare no competing interests.

Received: September 20, 2021
Revised: January 2, 2022
Accepted: January 14, 2022
Published: February 10, 2022; corrected online: February 24, 2022

REFERENCES

Agudelo, L.Z., Ferreira, D.M.S., Cervenka, I., Bryzgalova, G., Dadvar, S., Jannig, P.R., Pettersson-Klein, A.T., Lakshmikanth, T., Sustarsic, E.G., Porsmyr-Palmertz, M., et al. (2018). Kynurenic acid and Gpr35 regulate adipose tissue energy homeostasis and inflammation. Cell Metab *27*, 378–392.e5.

Ajuebor, M.N., Das, A.M., Virág, L., Flower, R.J., Szabó, C., and Perretti, M. (1999). Role of resident peritoneal macrophages and mast cells in chemokine production and neutrophil migration in acute inflammation: evidence for an inhibitory loop involving endogenous IL-10. J. Immunol. *162*, 1685–1691.

Askenase, P.W., Bursztajn, S., Gershon, M.D., and Gershon, R.K. (1980). T cell-dependent mast cell degranulation and release of serotonin in murine delayed-type hypersensitivity. J. Exp. Med. *152*, 1358–1374.

Askenase, P.W., Van Loveren, H., Kraeuter-Kops, S., Ron, Y., Meade, R., Theoharides, T.C., Nordlund, J.J., Scovern, H., Gerhson, M.D., and Ptak, W. (1983). Defective elicitation of delayed-type hypersensitivity in W/Wv and Sl/Sld mast cell-deficient mice. J. Immunol. *131*, 2687–2694.

Barth, M.C., Ahluwalia, N., Anderson, T.J., Hardy, G.J., Sinha, S., Alvarez-Cardona, J.A., Pruitt, I.E., Rhee, E.P., Colvin, R.A., and Gerszten, R.E. (2009). Kynurenic acid triggers firm arrest of leukocytes to vascular endothelium under flow conditions. J. Biol. Chem. *284*, 19189–19195.

Bengel, D., Murphy, D.L., Andrews, A.M., Wichems, C.H., Feltner, D., Heils, A., Mössner, R., Westphal, H., and Lesch, K.P. (1998). Altered brain serotonin homeostasis and locomotor insensitivity to 3, 4-methylenedioxymethamphetamine ("Ecstasy") in serotonin transporter-deficient mice. Mol. Pharmacol. *53*, 649–655.

Berger, M., Gray, J.A., and Roth, B.L. (2009). The expanded biology of serotonin. Annu. Rev. Med. *60*, 355–366.

Bogoslowski, A., Butcher, E.C., and Kubes, P. (2018). Neutrophils recruited through high endothelial venules of the lymph nodes via PNAd intercept disseminating Staphylococcus aureus. Proc. Natl. Acad. Sci. USA *115*, 2449–2454.

Boleij, A., Fathi, P., Dalton, W., Park, B., Wu, X., Huso, D., Allen, J., Besharati, S., Anders, R.A., Housseau, F., et al. (2021). G-protein coupled receptor 35 (GPR35) regulates the colonic epithelial cell response to enterotoxigenic Bacteroides fragilis. Commun. Biol. *4*, 585.

Bortolato, M., Chen, K., and Shih, J.C. (2008). Monoamine oxidase inactivation: from pathophysiology to therapeutics. Adv. Drug Deliv. Rev. *60*, 1527–1533.

Bortolato, M., Chen, K., and Shih, J.C. (2010). The degradation of serotonin: role of MAO. In Handbook of Behavioral Neurobiology of Serotonin, C. Miller and B. Jacobs, eds. (Elsevier), pp. 203–218.

Buscher, K., Wang, H., Zhang, X., Striewski, P., Wirth, B., Saggu, G., Lütke-Enking, S., Mayadas, T.N., Ley, K., Sorokin, L., et al. (2016). Protection from septic peritonitis by rapid neutrophil recruitment through omental high endothelial venules. Nat. Commun. *7*, 10828.

Callebert, J., Esteve, J.M., Hervé, P., Peoc'h, K., Tournois, C., Drouet, L., Launay, J.M., and Maroteaux, L. (2006). Evidence for a control of plasma serotonin levels by 5-hydroxytryptamine(2B) receptors in mice. J. Pharmacol. Exp. Ther. *317*, 724–731.

Cheong, J.E., and Sun, L. (2018). Targeting the IDO1/TDO2-KYN-AhR pathway for cancer immunotherapy - challenges and opportunities. Trends Pharmacol. Sci. *39*, 307–325.

Cloutier, N., Paré, A., Farndale, R.W., Schumacher, H.R., Nigrovic, P.A., Lacroix, S., and Boilard, E. (2012). Platelets can enhance vascular permeability. Blood *120*, 1334–1343.

Côté, F., Thévenot, E., Fligny, C., Fromes, Y., Darmon, M., Ripoche, M.A., Bayard, E., Hanoun, N., Saurini, F., Lechat, P., et al. (2003). Disruption of the nonneuronal tph1 gene demonstrates the importance of peripheral serotonin in cardiac function. Proc. Natl. Acad. Sci. USA *100*, 13525–13530.

Deng, H., Hu, H., and Fang, Y. (2012). Multiple tyrosine metabolites are GPR35 agonists. Sci. Rep. *2*, 373.

Deppermann, C., and Kubes, P. (2018). Start a fire, kill the bug: the role of platelets in inflammation and infection. Innate Immun *24*, 335–348.

Divorty, N., Milligan, G., Graham, D., and Nicklin, S.A. (2018). The orphan receptor GPR35 contributes to angiotensin II-induced hypertension and cardiac dysfunction in mice. Am. J. Hypertens. *31*, 1049–1058.

Duerschmied, D., Suidan, G.L., Demers, M., Herr, N., Carbo, C., Brill, A., Cifuni, S.M., Mauler, M., Cicko, S., Bader, M., et al. (2013). Platelet serotonin promotes the recruitment of neutrophils to sites of acute inflammation in mice. Blood *121*, 1008–1015.

Eisa, M., Tefera, K., and Alvanpour, A. (2018). Listeria peritonitis and bacteremia in a patient with cholangiocarcinoma. IDCases. ID *14*, e00430.

Enerbäck, L. (1963). Serotonin in human mast cells. Nature *197*, 610–611.

Etzioni, A. (2009). Genetic etiologies of leukocyte adhesion defects. Curr. Opin. Immunol. *21*, 481–486.

Facciorusso, A., Antonino, M., Orsitto, E., and Sacco, R. (2019). Primary and secondary prophylaxis of spontaneous bacterial peritonitis: current state of the art. Expert Rev. Gastroenterol. Hepatol. *13*, 751–759.

Farooq, S.M., Hou, Y., Li, H., O'Meara, M., Wang, Y., Li, C., and Wang, J.M. (2018). Disruption of GPR35 exacerbates dextran sulfate sodium-induced colitis in mice. Dig. Dis. Sci. *63*, 2910–2922.

Filippi, M.D. (2019). Neutrophil transendothelial migration: updates and new perspectives. Blood *133*, 2149–2158.

Foata, F., Sprenger, N., Rochat, F., and Damak, S. (2020). Activation of the G-protein coupled receptor GPR35 by human milk oligosaccharides through different pathways. Sci. Rep. *10*, 16117.

Freitag, A., Wessler, I., and Racke, K. (1995). Characterization of 5-hydroxytryptamine release from isolated rabbit and rat trachea: the role of neuroendocrine epithelia cells and mast cells. Naunyn Schmiedebergs Arch. Pharmacol. *353*, 55–63.

Galli, S.J., Gaudenzio, N., and Tsai, M. (2020). Mast cells in inflammation and disease: recent progress and ongoing concerns. Annu. Rev. Immunol. *38*, 49–77.

Gealageas, R., Devineau, A., So, P.P.L., Kim, C.M.J., Surendradoss, J., Buchwalder, C., Heller, M., Goebeler, V., Dullaghan, E.M., Grierson, D.S., et al. (2018). Development of novel monoamine oxidase-B (MAO-B) inhibitors with reduced blood-brain barrier permeability for the potential management of noncentral nervous system (CNS) diseases. J. Med. Chem. *61*, 7043–7064.

Geba, G.P., Ptak, W., Anderson, G.M., Paliwal, V., Ratzlaff, R.E., Levin, J., and Askenase, P.W. (1996). Delayed-type hypersensitivity in mast cell-deficient

mice: dependence on platelets for expression of contact sensitivity. J. Immunol. *157*, 557–565.

Gershon, R.K., Askenase, P.W., and Gershon, M.D. (1975). Requirement for vasoactive amines for production of delayed-type hypersensitvity skin reactions. J. Exp. Med. *142*, 732–747.

Girbl, T., Lenn, T., Perez, L., Rolas, L., Barkaway, A., Thiriot, A., Del Fresno, C., Lynam, E., Hub, E., Thelen, M., et al. (2018). Distinct compartmentalization of the chemokines CXCL1 and CXCL2 and the atypical receptor ACKR1 determine discrete stages of neutrophil diapedesis. Immunity *49*, 1062–1076.e6.

Gros, A., Syvannarath, V., Lamrani, L., Ollivier, V., Loyau, S., Goerge, T., Nieswandt, B., Jandrot-Perrus, M., and Ho-Tin-Noé, B. (2015). Single platelets seal neutrophil-induced vascular breaches via GPVI during immune-complex-mediated inflammation in mice. Blood *126*, 1017–1026.

Herr, N., Bode, C., and Duerschmied, D. (2017). The effects of serotonin in immune cells. Front. Cardiovasc. Med. *4*, 48.

Herstowska, M., Komorowska, O., Cubała, W.J., Jakuszkowiak-Wojten, K., Gałuszko-Węgielnik, M., and Landowski, J. (2014). Severe skin complications in patients treated with antidepressants: a literature review. Postepy Dermatol. Alergol. *31*, 92–97.

Jackson-Jones, L.H., Smith, P., Portman, J.R., Magalhaes, M.S., Mylonas, K.J., Vermeren, M.M., Nixon, M., Henderson, B.E.P., Dobie, R., Vermeren, S., et al. (2020). Stromal cells covering omental fat-associated lymphoid clusters trigger formation of neutrophil aggregates to capture peritoneal contaminants. Immunity *52*, 700–715.e6.

Jarchum, I., Liu, M., Shi, C., Equinda, M., and Pamer, E.G. (2012). Critical role for MyD88-mediated neutrophil recruitment during Clostridium difficile colitis. Infect. Immun. *80*, 2989–2996.

Jenkins, L., Alvarez-Curto, E., Campbell, K., de Munnik, S., Canals, M., Schlyer, S., and Milligan, G. (2011). Agonist activation of the G protein-coupled receptor GPR35 involves transmembrane domain III and is transduced via $G\alpha_{13}$ and β-arrestin-2. Br. J. Pharmacol. *162*, 733–748.

Karhausen, J., Choi, H.W., Maddipati, K.R., Mathew, J.P., Ma, Q., Boulaftali, Y., Lee, R.H., Bergmeier, W., and Abraham, S.N. (2020). Platelets trigger perivascular mast cell degranulation to cause inflammatory responses and tissue injury. Sci. Adv. *6*, eaay6314.

Kaya, B., Donas, C., Wuggenig, P., Diaz, O.E., Morales, R.A., Melhem, H., Swiss, I.B.D.C.I., Hernandez, P.P., Kaymak, T., Das, S., et al. (2020). Lysophosphatidic acid-mediated GPR35 signaling in CX3CR1(+) macrophages regulates intestinal homeostasis. Cell Rep *32*, 107979.

Kornerup, K.N., Salmon, G.P., Pitchford, S.C., Liu, W.L., and Page, C.P. (2010). Circulating platelet-neutrophil complexes are important for subsequent neutrophil activation and migration. J. Appl. Physiol. *109* (1985), 758–767.

Kubes, P., and Gaboury, J.P. (1996). Rapid mast cell activation causes leukocyte-dependent and -independent permeability alterations. Am. J. Physiol. *271*, H2438–H2446.

Kushnir-Sukhov, N.M., Brown, J.M., Wu, Y., Kirshenbaum, A., and Metcalfe, D.D. (2007). Human mast cells are capable of serotonin synthesis and release. J. Allergy Clin. Immunol. *119*, 498–499.

Lefrançais, E., Mallavia, B., Zhuo, H., Calfee, C.S., and Looney, M.R. (2018). Maladaptive role of neutrophil extracellular traps in pathogen-induced lung injury. JCI Insight *3*, e98178.

Lefrançais, E., Ortiz-Muñoz, G., Caudrillier, A., Mallavia, B., Liu, F., Sayah, D.M., Thornton, E.E., Headley, M.B., David, T., Coughlin, S.R., et al. (2017). The lung is a site of platelet biogenesis and a reservoir for haematopoietic progenitors. Nature *544*, 105–109.

Lehtosalo, J.I., Uusitalo, H., Laakso, J., Palkama, A., and Härkönen, M. (1984). Biochemical and immunohistochemical determination of 5-hydroxytryptamine located in mast cells in the trigeminal ganglion of the rat and guinea pig. Histochemistry *80*, 219–223.

Lindström, M., Tohmola, N., Renkonen, R., Hämäläinen, E., Schalin-Jäntti, C., and Itkonen, O. (2018). Comparison of serum serotonin and serum 5-HIAA LC-MS/MS assays in the diagnosis of serotonin producing neuroendocrine neoplasms: a pilot study. Clin. Chim. Acta *482*, 78–83.

Lu, E., Wolfreys, F.D., Muppidi, J.R., Xu, Y., and Cyster, J.G. (2019). S-geranylgeranyl-L-glutathione is a ligand for human B cell-confinement receptor P2RY8. Nature *567*, 244–248.

Maas, S.L., Soehnlein, O., and Viola, J.R. (2018). Organ-specific mechanisms of transendothelial neutrophil migration in the lung, liver, kidney, and aorta. Front. Immunol. *9*, 2739.

Mackenzie, A.E., Quon, T., Lin, L.C., Hauser, A.S., Jenkins, L., Inoue, A., Tobin, A.B., Gloriam, D.E., Hudson, B.D., and Milligan, G. (2019). Receptor selectivity between the G proteins $G\alpha12$ and $G\alpha13$ is defined by a single leucine-to-isoleucine variation. FASEB J *33*, 5005–5017.

Manne, B.K., Denorme, F., Middleton, E.A., Portier, I., Rowley, J.W., Stubben, C., Petrey, A.C., Tolley, N.D., Guo, L., Cody, M., et al. (2020). Platelet gene expression and function in patients with COVID-19. Blood *136*, 1317–1329.

Meixiong, J., Anderson, M., Limjunyawong, N., Sabbagh, M.F., Hu, E., Mack, M.R., Oetjen, L.K., Wang, F., Kim, B.S., and Dong, X. (2019). Activation of mast-cell-expressed mas-related G-protein-coupled receptors drives non-histaminergic itch. Immunity *50*, 1163–1171.e5.

Morishima, T. (1970). 5-Hydroxytryptamine (serotonin) and 5-hydroxytryptophan in mast cells of human mastocytosis. Tohoku J. Exp. Med. *102*, 121–126.

Musgrave, T., Benson, C., Wong, G., Browne, I., Tenorio, G., Rauw, G., Baker, G.B., and Kerr, B.J. (2011). The MAO inhibitor phenelzine improves functional outcomes in mice with experimental autoimmune encephalomyelitis (EAE). Brain Behav. Immun. *25*, 1677–1688.

Muzumdar, M.D., Tasic, B., Miyamichi, K., Li, L., and Luo, L. (2007). A global double-fluorescent Cre reporter mouse. Genesis *45*, 593–605.

Nourshargh, S., and Alon, R. (2014). Leukocyte migration into inflamed tissues. Immunity *41*, 694–707.

Nowak, E.C., de Vries, V.C., Wasiuk, A., Ahonen, C., Bennett, K.A., Le Mercier, I., Ha, D.G., and Noelle, R.J. (2012). Tryptophan hydroxylase-1 regulates immune tolerance and inflammation. J. Exp. Med. *209*, 2127–2135.

Ohshiro, H., Tonai-Kachi, H., and Ichikawa, K. (2008). GPR35 is a functional receptor in rat dorsal root ganglion neurons. Biochem. Biophys. Res. Commun. *365*, 344–348.

Oka, S., Ota, R., Shima, M., Yamashita, A., and Sugiura, T. (2010). GPR35 is a novel lysophosphatidic acid receptor. Biochem. Biophys. Res. Commun. *395*, 232–237.

Pagano, E., Elias, J.E., Schneditz, G., Saveljeva, S., Holland, L.M., Borrelli, F., Karlsen, T.H., Kaser, A., and Kaneider, N.C. (2021). Activation of the GPR35 pathway drives angiogenesis in the tumour microenvironment. Gut. https://doi.org/10.1136/gutjnl-2020-323363.

Page, C., and Pitchford, S. (2013). Neutrophil and platelet complexes and their relevance to neutrophil recruitment and activation. Int. Immunopharmacol. *17*, 1176–1184.

Park, S.J., Lee, S.J., Nam, S.Y., and Im, D.S. (2018). GPR35 mediates Lodoxamide-induced migration inhibitory response but not CXCL17-induced migration stimulatory response in THP-1 cells; is GPR35 a receptor for CXCL17? Br. J. Pharmacol. *175*, 154–161.

Pietraszek, M.H., Takahashi, S., Takada, Y., Ohara, K., Inatomi, H., Kondo, N., Ohara, K., and Takada, A. (1991). Diurnal patterns of serotonin, 5-hydroxyindoleacetic acid, tryptophan and fibrinolytic activity in blood of depressive patients and healthy volunteers. Thromb. Res. *64*, 243–252.

Pletscher, A. (1968). Metabolism, transfer and storage of 5-hydroxytryptamine in blood platelets. Br. J. Pharmacol. Chemother. *32*, 1–16.

Plum, T., Wang, X., Rettel, M., Krijgsveld, J., Feyerabend, T.B., and Rodewald, H.R. (2020). Human mast cell proteome reveals unique lineage, putative functions, and structural basis for cell ablation. Immunity *52*, 404–416.e5.

Poulsen, H.B., Steig, T.Á., Björkman, J.T., and Gaini, S. (2018). Peritonitis with *Listeria monocytogenes* in a patient on automated peritoneal dialysis. BMJ Case Rep *2018*, bcr2017220088.

Quon, T., Lin, L.C., Ganguly, A., Tobin, A.B., and Milligan, G. (2020). Therapeutic opportunities and challenges in targeting the orphan G protein-coupled receptor GPR35. ACS Pharmacol. Transl. Sci. *3*, 801–812.

Rogers, M.A., Greene, M.T., Young, V.B., Saint, S., Langa, K.M., Kao, J.Y., and Aronoff, D.M. (2013). Depression, antidepressant medications, and risk of Clostridium difficile infection. BMC Med *11*, 121.

Rossaint, J., Kühne, K., Skupski, J., Van Aken, H., Looney, M.R., Hidalgo, A., and Zarbock, A. (2016). Directed transport of neutrophil-derived extracellular vesicles enables platelet-mediated innate immune response. Nat. Commun. *7*, 13464.

Rosser, E.C., Piper, C.J.M., Matei, D.E., Blair, P.A., Rendeiro, A.F., Orford, M., Alber, D.G., Krausgruber, T., Catalan, D., Klein, N., et al. (2020). Microbiota-derived metabolites suppress arthritis by amplifying aryl-hydrocarbon receptor activation in regulatory B cells. Cell Metab *31*, 837–851.e10.

Sano, H., Suzuki, Y., Yazaki, R., Tamefusa, K., Ohara, K., Yokoyama, T., Miyasato, K., and Ohara, K. (1993). Circadian variation in plasma 5-hydroxyindoleacetic acid level during and after alcohol withdrawal: phase advances in alcoholic patients compared with normal subjects. Acta Psychiatr. Scand. *87*, 291–296.

Schmid, T., Snoek, L.B., Fröhli, E., van der Bent, M.L., Kammenga, J., and Hajnal, A. (2015). Systemic regulation of RAS/MAPK signaling by the serotonin metabolite 5-HIAA. PLOS Genet *11*, e1005236.

Schneditz, G., Elias, J.E., Pagano, E., Zaeem Cader, M., Saveljeva, S., Long, K., Mukhopadhyay, S., Arasteh, M., Lawley, T.D., Dougan, G., et al. (2019). GPR35 promotes glycolysis, proliferation, and oncogenic signaling by engaging with the sodium potassium pump. Sci. Signal. *12*, eaau9048.

Schwartz, J.T., Bandyopadhyay, S., Kobayashi, S.D., McCracken, J., Whitney, A.R., Deleo, F.R., and Allen, L.A. (2013). *Francisella tularensis* alters human neutrophil gene expression: insights into the molecular basis of delayed neutrophil apoptosis. J. Innate Immun. *5*, 124–136.

Schwartz, L.B. (1987). Mediators of human mast cells and human mast cell subsets. Ann. Allergy *58*, 226–235.

Shad, K.F., and Saeed, S.A. (2007). The metabolism of serotonin in neuronal cells in culture and platelets. Exp. Brain Res. *183*, 411–416.

Sjoerdsma, A., Waalkes, T.P., and Weissbach, H. (1957). Serotonin and histamine in mast cells. Science *125*, 1202–1203.

Slaba, I., and Kubes, P. (2017). Platelets and immunity. In Platelets in Thrombotic and Non-Thrombotic Disorders: Pathophysiology, Pharmacology and Therapeutics: an Update, P. Gresele, N.S. Kleiman, J.A. Lopez, and C.P. Page, eds. (Springer International Publishing)), pp. 489–512.

Slaba, I., Wang, J., Kolaczkowska, E., McDonald, B., Lee, W.Y., and Kubes, P. (2015). Imaging the dynamic platelet-neutrophil response in sterile liver injury and repair in mice. Hepatology *62*, 1593–1605.

Sonoda, H., Aoki, J., Hiramatsu, T., Ishida, M., Bandoh, K., Nagai, Y., Taguchi, R., Inoue, K., and Arai, H. (2002). A novel phosphatidic acid-selective phospholipase A1 that produces lysophosphatidic acid. J. Biol. Chem. *277*, 34254–34263.

Strydom, N., and Rankin, S.M. (2013). Regulation of circulating neutrophil numbers under homeostasis and in disease. J. Innate Immun. *5*, 304–314.

Tablang, M.V. (2008). Spontaneous bacterial peritonitis caused by infection with *Listeria monocytogenes*. Case Rep. Gastroenterol. *2*, 321–325.

Tanaka, T., Mori, M., Sekino, M., Higashijima, U., Takaki, M., Yamashita, Y., Kakiuchi, S., Tashiro, M., Morimoto, K., Tasaki, O., et al. (2021). Impact of plasma 5-hydroxyindoleacetic acid, a serotonin metabolite, on clinical outcome in septic shock, and its effect on vascular permeability. Sci. Rep. *11*, 14146.

Taniguchi, Y., Tonai-Kachi, H., and Shinjo, K. (2006). Zaprinast, a well-known cyclic guanosine monophosphate-specific phosphodiesterase inhibitor, is an agonist for GPR35. FEBS Lett *580*, 5003–5008.

Theoharides, T.C., Bondy, P.K., Tsakalos, N.D., and Askenase, P.W. (1982). Differential release of serotonin and histamine from mast cells. Nature *297*, 229–231.

Tohmola, N., Itkonen, O., Sane, T., Markkanen, H., Joenväärä, S., Renkonen, R., and Hämäläinen, E. (2014). Analytical and preanalytical validation of a new mass spectrometric serum 5-hydroxyindoleacetic acid assay as neuroendocrine tumor marker. Clin. Chim. Acta *428*, 38–43.

Tsukahara, T., Hamouda, N., Utsumi, D., Matsumoto, K., Amagase, K., and Kato, S. (2017). G protein-coupled receptor 35 contributes to mucosal repair in mice via migration of colonic epithelial cells. Pharmacol. Res. *123*, 27–39.

Wang, J., Simonavicius, N., Wu, X., Swaminath, G., Reagan, J., Tian, H., and Ling, L. (2006). Kynurenic acid as a ligand for orphan G protein-coupled receptor GPR35. J. Biol. Chem. *281*, 22021–22028.

Wernersson, S., and Pejler, G. (2014). Mast cell secretory granules: armed for battle. Nat. Rev. Immunol. *14*, 478–494.

Wirthgen, E., Hoeflich, A., Rebl, A., and Günther, J. (2018). Kynurenic acid: the Janus-faced role of an immunomodulatory tryptophan metabolite and its link to pathological conditions. Front. Immunol. *8*, 1957.

Xie, X., Shi, Q., Wu, P., Zhang, X., Kambara, H., Su, J., Yu, H., Park, S.Y., Guo, R., Ren, Q., et al. (2020). Single-cell transcriptome profiling reveals neutrophil heterogeneity in homeostasis and infection. Nat. Immunol. *21*, 1119–1133.

Yabut, J.M., Desjardins, E.M., Chan, E.J., Day, E.A., Leroux, J.M., Wang, B., Crane, E.D., Wong, W., Morrison, K.M., Crane, J.D., et al. (2020). Genetic deletion of mast cell serotonin synthesis prevents the development of obesity and insulin resistance. Nat. Commun. *11*, 463.

Zarbock, A., Singbartl, K., and Ley, K. (2006). Complete reversal of acid-induced acute lung injury by blocking of platelet-neutrophil aggregation. J. Clin. Invest. *116*, 3211–3219.

Zhao, P., Sharir, H., Kapur, A., Cowan, A., Geller, E.B., Adler, M.W., Seltzman, H.H., Reggio, P.H., Heynen-Genel, S., Sauer, M., et al. (2010). Targeting of the orphan receptor GPR35 by pamoic acid: a potent activator of extracellular signal-regulated kinase and beta-arrestin2 with antinociceptive activity. Mol. Pharmacol. *78*, 560–568.

STAR★METHODS

KEY RESOURCES TABLE

REAGENT or RESOURCE	SOURCE	IDENTIFIER
Antibodies		
FITC-conjugated rat anti-mouse Ly6C (AL-21)	BD	#553104; RRID:AB_394628
APC-Cy7-conjugated rat anti-mouse Ly6G (1A8)	TONBO	#25-1276-U100; RRID:AB_2621632
BV785-conjugated rat anti-mouse CD11b (M1/70,	BioLegend	#101243; RRID:AB_2561373
APC-conjugated rat anti-mouse CXCR2 (SA044G4)	BioLegend	#149312; RRID:AB_2728185
FITC-conjugated rat anti-mouse CD45.2 antibody (104)	BioLegend	#109805; RRID:AB_313442
PE-conjugated rat anti-mouse CD45.1 (A20)	BioLegend	#110708; RRID:AB_313497
FITC-conjugated rat anti-mouse CD11a (I21/7)	BioLegend	#153105; RRID:AB_2716035
Biotin-conjugated rat-anti mouse CD18 (C71/16)	BD	#557439; RRID:AB_396702
FITC-conjugated rat anti mouse LFA-1 (REA880)	Miltenyi Biotec	#130-114-422; RRID:AB_2726624
PE-Cy7-conjugated rat anti-mouse CD62L (Mel-14)	BioLegend	#104418; RRID:AB_313103
BV421-conjugated rat anti-mouse PSGL1 (2PH1)	BD	#562807; RRID:AB_2737808
PE-conjugated rat anti-mouse CD117 (2B8)	Fisher	#553355; RRID:AB_394806
FITC-conjugated rat anti-mouse CD63 (NVG-2)	BioLegend	#143920; RRID:AB_2876488
PE- conjugated anti-mouse CD45.2 (104)	BioLegend	#109808; RRID:AB_313445
Biotinylated OX56 antibody	Bio X Cell	In house
AF647-conjugated anti-mouse/rat CD90.1	BioLegend	#202508; RRID:AB_492884
Streptavidin–PE	BioLegend	#405203
Rabbit polyclonal anti-mouse GPR35	Biomatik	#2314-AP106RI
AF647-Goat anti-Rabbit IgG (H+L) Highly Cross-Adsorbed Ab	Fisher Scientific	#A21245; RRID:AB_141775
FITC- conjugated rat anti-mouse CD41 (MWReg30)	BioLegend	#133903; RRID:AB_1626237
anti-5-HIAA polyclonal	My-Bio-Source	#MBS2032649
Bacterial and virus strains		
Listeria monocytogenes	A gift from D. Portnoy, UC Berkley	N/A
E.coli (K1)	A gift from Dr. Matthay, UCSF	N/A
Chemicals, peptides, and recombinant proteins		
Lodoxamide	Sigma	#SML2307
Kynurenic acid	Sigma	#K3375
18:1 LPA	Sigma	#L7260
5-HIAA	Sigma	#H8876
Serotonin	Cayman Chemical	#14332
PTX	List Biological Labs, Inc	#181
Diptheria Toxin	Millipore	#322326
Critical commercial assays		
Mouse 5-Hydroxyindoleacetic acid (5HIAA 5-HIAA) ELISA Kit	AssayGenie	# MOEB2528
Deposited data		
Murine neutrophil data	Xie et al., 2020	GSE137540
Human neutrophil data	Schwartz et al., 2013	BioGps
Experimental models: Cell lines		
WEHI-231	Cell line was previously obtained from other laboratories and further authentication was not performed.	N/A

(*Continued on next page*)

Continued

REAGENT or RESOURCE	SOURCE	IDENTIFIER
bEND3	Cell line was previously obtained from other laboratories and further authentication was not performed.	N/A
HEK293T (Platinum-E (Plat-E) Retroviral Packaging Cell Line)	Gift from S. Schwab, NYU	N/A
Experimental models: Organisms/strains		
C57BL/6J	Jackson Laboratories	#000664
B6.SJL-Ptprca Pepcb/BoyJ	Jackson Laboratories	#002014
Gpr35−/−	EMMA (EM09677; Gpr35tm1b(EUCOMM)Hmgu)	N/A
Pf4-Cre x mTmG (Gt(ROSA)26Sortm4 (ACTB-tdTomato,-EGFP)Luo/J)	Looney lab, UCSF (Lefrançais et al., 2017)	N/A
Mrp8-Cre x mTmG	Looney lab, UCSF (Lefrançais et al., 2018)	N/A
Kit/v x Kit/W	Jackson Laboratories	#100410
B6.129(Cg)-Slc6a4tm1Kpl/J	Jackson Laboratories	#008355
Tph1 Het and KO Bone Marrow	Waliul Khan lab, McMaster Univ. (Cote et al., 2003)	N/A
Oligonucleotides		
CTGGACGAGTCGGTCAGAAG-Fwd (Gpr35 qPCR)	N/A	N/A
GCGTTGGAAAGATTCGCCTTT-Rev (Gpr35 qPCR)	N/A	N/A
Recombinant DNA		
MSCV-IRES-Thy1.1	Addgene	Plasmid ID: 17442
MSCV-IRES-GFP	Addgene	Plasmid ID: 20672
Software and algorithms		
IMARIS (v.9.6.0)	Imaris softawre	https://imaris.oxinst.com/
Flowjo (v.10.6.2)	Flowjo	https://www.flowjo.com/
Prism (GraphPad 9.0.1)	GraphPad software	https://www.graphpad.com/scientific-software/prism/
Seurat R package (version 2.2)	Seurat	https://satijalab.org/seurat/
R studio (3.5)	R software	https://www.rstudio.com/
Adobe Illustrator CS6	Adobe System	N/A

RESOURCE AVAILABILITY

Lead contact

Further information and requests for reagents may be directed to and will be fulfilled by the lead contact Jason Cyster (jason.cyster@ucsf.edu).

Materials availability

Further information and requests for reagents will be fulfilled by Dr. Jason Cyster (jason.cyster@ucsf.edu). A list of critical reagents (key resources) is included in the key resources table. Some material may require requests to collaborators and/or agreements with various entities. Material that can be shared will be released via a Material Transfer Agreement.

Data and code availability

All data reported in this paper will be shared by the lead contact upon request.

This paper does not report original code.

Any additional information required to reanalyze the data reported in this paper is available from the lead contact upon request.

EXPERIMENTAL MODEL AND SUBJECT DETAILS

Mice

C57BL/6J and BoyJ (CD45.1) mice were bred in an internal colony and 7–12-week-old mice of both sexes were used. Gpr35$^{-/-}$ mice were obtained from EMMA (EM09677; Gpr35tm1b(EUCOMM)Hmgu) and maintained on a B6 background. C57BL/6-Gt(ROSA)26Sortm1(HBEGF)Awai/J (iDTR mice) were purchased from Jackson Laboratories. Platelet-deficient mice (c-mpl$^{-/-}$), Pf4-Cre x mTmG (Gt(ROSA)26Sor$^{tm4(ACTB-tdTomato,-EGFP)Luo}$/J) platelet reporter mice (Lefrançais et al., 2017) and Mrp8-Cre x mTmG neutrophil reporter mice (Lefrançais et al., 2018) were all on a B6 background. Mast cell-deficient Kit/v x Kit/W mice and SERT-deficient mice (Bengel et al., 1998) were obtained from Jackson Laboratories and maintained on a B6 background. Tph1 KO (Côté et al., 2003) BM was provided by Huaquing Wang and Waliul Khan (McMaster Univ.). Littermate controls (WT and HET) were used for experiments, mice were allocated to control and experimental groups randomly, sample sizes were chosen based on previous experience to obtain reproducible results and the investigators were not blinded.

METHOD DETAILS

Treatments and bone marrow chimeras

In co-transfer experiments, purified WT and KO neutrophils were stained for 30 min at 37°C with Cell trace Violet (#C34557, Fisher), CMTMR (#C2927, ThermoFisher), CFSE (#C34554, ThermoFisher), or Deep red (#C34565, Life Tech) as indicated and mixed 50:50 before injection (0.5-3 x 10^7 neutrophil / mouse in 200ul saline), 30 min before i.p. TG. To induce peritonitis, mice were injected i.p. with either 1ml of thioglycolate 4% (Sigma), 500ng TNF in 500μl saline (Biolegend) or 1x10^5 CFUs *Listeria* or 1x10^4 CFUs *E.coli* in 500μl saline. To stimulate neutrophil recruitment to draining LNs, mice were s.c. injected with 5 x 10^6 CFUs in 40μl saline. To boost neutrophil homing to the skin, anesthetized mice were ear-pricked (20 time/ear) with *Listeria*-contaminated needles (27G). To deplete platelet 5-HIAA, mice were treated for 3 weeks with Fluoxetine (160mg/L dissolved in drinking water, #1279804, Millipore Sigma) before skin-pricking, similarly to what has been previously reported (Cloutier et al., 2012; Musgrave et al., 2011). To deplete total generation of 5-HIAA, mice were treated with two i.p. doses of Phenelzine (30mg/kg, #P6777, Millipore Sigma) at -18hr and -1hr before skin-pricking. To disrupt 5-HIAA or Kynurenic acid *in vivo* gradients, 200μl saline containing 100μM 5-HIAA or Kynurenic acid (Sigma) were injected i.v. 10 min before i.p. TNF treatment. To produce mixed chimeras, CD45.1 congenic Boy/J mice were lethally irradiated with 1300 rad in split doses and reconstituted with 5 × 10^6 BM cells (~50:50) as indicated. Mice were analyzed 6–7 weeks later. Animals were housed in a pathogen-free environment in the Laboratory Animal Resource Center at the University of California, San Francisco, and all experiments conformed to ethical principles and guidelines that were approved by the Institutional Animal Care and Use Committee. To generate mice with full GPR35-deficiency restricted to neutrophils, MRP8-Cre x iDTR BM was mixed 1:1 with GPR35 WT or KO BM and used to reconstitute WT mice. After 6 weeks reconstitution the chimeras were treated with 400ng diptheria toxin i.v. (DT) at d-1 and with 80ng DT i.v. 2hr before infection with *Listeria*. iDTR-expressing neutrophil depletion was confirmed by flow cytometry. To deplete platelets, mice were treated with 2ug/g of anti-CD42b depleting antibody (Emfret Analytics) 24 hr before the experiment. Platelet-deficient or platelet-depleted mice showed extensive peritoneal bleeding after i.p. TG or TNF injection, resulting in animals having to be euthanized within 12-18hrs after injection. Therefore, all data with platelet deficient or depleted mice were obtained using the skin model. To locally activate mast cells, 50μl of compound 48/80 (50μg/ml, Sigma) were injected s.c. 5 min before *Listeria* pricking. In indicated experiments, mast cell-deficient mice were injected s.c.with 2uM 5-HIAA (or DMSO) in 20ul in the ear skin immediately before *Listeria* skin-pricking.

Flow cytometry and cell sorting

Neutrophils were identified as either Ly6G$^+$ Ly6C$^+$ CD11b$^+$ or Ly6G$^+$ CD11b$^+$ cells as indicated, using the following antibodies: fluorescein isothiocyanate (FITC)-conjugated rat anti-mouse Ly6C (AL-21, #553104, BD); APC-Cy7-conjugated rat anti-mouse Ly6G (1A8, TONBO); BV785-conjugated rat anti-mouse CD11b (M1/70, #101243, BioLegend) and APC-conjugated rat anti-mouse CXCR2 (SA044G4, #149312, BioLegend). PE rat anti-mouse CD45.1 (A20, 110708, Biolegend) and FITC rat anti-mouse CD45.2 antibody (104,109805, BioLegend). FITC-conjugated rat anti-mouse CD11a (I21/7, #153105, BioLegend); Biotin-conjugated rat-anti mouse CD18 (C71/16, #557439, BD); FITC-conjugated rat anti mouse LFA-1 (REA880, #130-114-422, Miltenyi Biotec); APC-conjugated rat anti-mouse CXCR2 (SA044G4, #149311, BioLegend); PE-Cy7-conjugated rat anti-mouse CD62L (Mel-14, #104418, BioLegend); BV421-conjugated rat anti-mouse PSGL1 (2PH1, #562807, BD). To analyze mast cells, PE-conjugated rat anti-mouse CD117 (2B8, #553355, Fisher) and FITC-conjugated rat anti-mouse CD63 (NVG-2, #143920, BioLegend) were used.

To identify intravascular cells, 2 μg / 200μl saline of PE- conjugated anti-mouse CD45.2 (104, #109808, Biolegend) were injected 2 min before sacrifice as indicated. For flow cytometry staining, cells were placed in a 96-well round bottom plate and washed with staining buffer (PBS containing 2% NBCS and 0.5 mM EDTA), and 40 μl of antibody cocktail was added to each sample for 20 min on ice. After incubation, cells were washed twice with staining buffer. For staining of the N-terminal OX56 tag, a 1:200 dilution of a biotinylated OX56 antibody (Bio X Cell) was placed on the cells for 25 min on ice, after which the cells were washed and a 1:200 dilution of streptavidin–PE (#405203, BioLegend) was incubated with the cells for 20 min. To identify Thy1.1 reporter expression, AF647-conjugated anti-mouse/rat CD90.1 (#202508) was used. Rabbit polyclonal anti-GPR35 was produced by Biomatik (using as immunogen the C terminus peptide: MAREFQEASKPATSSNTPHKSQDSQILSLT) and affinity-purified. To reduce staining background,

anti-GPR35 polyclonal antibody was pre-absorbed against GPR35 KO splenocytes overnight at 4°C. Cells were surface-stained, fixed and permeabilized (eBioscience™, #00552100) before intracellular staining. AF647-Goat anti-Rabbit IgG (H+L) Highly Cross-Adsorbed Ab (A21245, Fisher Scientific) was used as secondary antibody. To quantify neutrophil-platelet interaction, 100 μl of blood were obtained by retro-orbital bleeding (heparinized capillaries) and drawn into tubes containing 1ml of Lyse/Fix Buffer 5X (Ox-7, #558049, BioLegend) and incubated for 15 min. Cells were than wash and resuspended in staining buffer. FITC-conjugated anti-mouse CD41 (MWReg30, # 133903, BioLegend) was used to stain neutrophils that had acquired membrane-bound platelet. Data were acquired using a BD LSR II flow cytometer or a Cytek Aurora. A BD FACSAria II was used to sort murine $Ly6G^+$ $CD11b^+$ $CXCR2^+$ neutrophils (purity >96%). Flow cytometry data were analyzed using Flowjo (v.10.6.2).

Generation of GPR35-expressing WEHI-231 cells

Murine and human GPR35 were cloned into the murine stem cell virus (MSCV)-GFP retroviral vector (mGPR35-GFP or hGPR35-Thy1.1). The retroviruses encoding mGPR35-GFP/hGPR35-Thy1.1 were produced using the Platinum-E packaging cell line, as previously described (Lu et al., 2019). Briefly, 5×10^5 WEHI-231 cells were placed in a 6-well plate along with the retroviral supernatant and the cells were centrifuged at 1,340g (2,400 r.p.m.) for 2 h at room temperature. This spinfection was repeated with fresh retrovirus for a second time 24 h later. Then, 48 h after the second spinfection, the highest 3% of GFP/Thy1.1-expressing cells were sorted using a BD FACSAria II. These cells were combined with GFP/Thy1.1-negative cells in a ~1:1 ratio to run transwell migration assays.

Cell lines and treatments

HEK293T and bEND3 cells were grown in 10-cm tissue culture dishes in DMEM containing 10% FBS, 10 mM HEPES, 2 mM glutamine and 50 IU/L penicillin/streptomycin. WEHI-231 were grown in upright T25 flasks in RPMI containing 10% FBS, 10 mM HEPES, 2 mM glutamine, 55 μM 2-mercaptoethanol and 50 U penicillin/streptomycin. All cell lines were previously obtained from other laboratories and further authentication was not performed. The cell lines were not tested for mycoplasma contamination. To test the activity of 2-acyl LPA, empty vector (EV) or Lipase member H (LIPH)-transfected HEK293T cells were grown out in 10-cm tissue culture dishes and allowed to reach confluence. The medium was then replaced with serum-free medium (RPMI containing 0.5% fatty acid-free BSA and 10 mM HEPES) and tested in the bioassay. LIPH is also known as PA-PLA1 and it catalyzes removal of the sn-1 acyl chain from phosphatidic acid to generate 2-acyl LPA (Sonoda et al., 2002). For transfection of HEK293T cells, mouse *Liph* was cloned into an MSCV-Thy1.1 retroviral vector, similarly to what previously described (Lu et al., 2019). Briefly, HEK293T cells were seeded into 10-cm tissue culture dishes and grown until 75% confluent in antibiotic-free medium. Plasmids were aliquoted in Opti-MEM, then mixed with Lipofectamine 2000 (at 6 μl per 3 μg plasmid) and allowed to sit for 25 min at room temperature. The mixtures were gently added dropwise to the HEK293T cells. Then, 24 h after transfection, the medium was replaced with serum-free medium. To inhibit Gαi-signaling, GPR35-GFP and control WEHI-231 cells were pre-treated with 100ng/ml pertussis toxin (PTX, #181, List Biological Labs, Inc) for 30 min at 37°C before running the transwell migration assay. P815 mastocytoma cells were used as a mast cell-like cell line. To block 5-HIAA-driven migration, anti-5-HIAA polyclonal antibody (My-bio-Source) was used at 2ug/ml.

Chemicals and reagents

Lodoxamide (#SML2307), Kynurenic acid (#K3375), 18:1 LPA (#L7260), and 5-HIAA (#H8876) were purchased from Sigma. Serotonin (#14332) was purchased from Cayman Chemical.

Quantitative PCR

Total RNA from sorted BM, blood or peritoneal neutrophils was extracted using an RNeasy kit (Qiagen) and reverse-transcribed using M-MLV reverse transcriptase. qPCR was performed using Power SYBR Green with an Applied Biosystems StepOnePlus instrument. Data were analyzed with the comparative Ct ($2-\Delta\Delta Ct$) method, using the housekeeping genes indicated in the figures.

Transwell migration assay

Control and GPR35-transduced WEHI-231 cells were taken from T25 flask cultures, washed twice in pre-warmed migration medium (RPMI containing 0.5% fatty acid-free BSA, 10 mM HEPES and 50 IU/L penicillin/streptomycin) and mixed 50:50. The cells were resuspended in migration medium at 2×10^6 cells / ml and resensitized for 10 min in a 37 °C water bath in migration medium (0.5% fatty-acid free BSA, 10mM Hepes RPMI). Transwell filters (6 mm insert, 5 μm pore size, Corning) were placed on top of each well, and 100 μl containing 2×10^5 cells of GPR35–GFP/ control WEHI-231 cell mix was added to the transwell insert. The cells were allowed to migrate for 3 hr, after which the cells in the bottom well were counted by flow cytometry. For neutrophil transwell migration assay, peritoneal cells from WT-CD45.1 / GPR35 KO mixed chimeras (2hr after TG) were diluted at 2×10^6 cells / ml in 0.5% fatty-acid free BSA, 0.5% FBS (migration plus) medium. Preliminary experiments established that inclusion of a low amount of FBS was necessary to maintain viability of the neutrophils during the assay. Representative experiments for each migration assay are plotted as a percentage of input migration. The baseline migration between experiments differs based on the growth state of the WEHI-231 cells.

Transendothelial migration assay and adhesion assay

To perform a neutrophil *in vitro* transmigration assay, bEND3 cells were trypsinized and resuspended at $4\text{-}5x10^5$ / ml in complete medium. 24 well plate containing 0.6ml complete (10%FCS) medium per well were prepared, transwells (5um) were inserted in

the plates and 100ul of bEND3 cell mix were gently pipetted on each transwell (5um, Corning). Cells were allowed to grow on transwells for 48 hrs. Confluent bEND3-containing transwells were stimulated for 1hr with TNF (100ng/ml) before the assay. After activation, excess medium was removed, transwells were washed twice and placed in new 24-well plates containing indicated dilutions if migration stimuli. Peritoneal cells (2hr after TG) were diluted at $2x10^6$ / ml and 100ul of peritoneal cell mix in migration medium were gently pipetted on bEND3 transwells. Cells were allowed to migrate for 2hr at 37°C. Cells and migration stimuli were diluted in 0.5% FBS migration plus medium. Data are plotted as % of input migration. To perform neutrophil or WEHI-231 adhesion assays, $3x10^4$ bEND3 cells /well were seeded in flat 96 well plates for 24hr. Confluent bEND3-containing wells were stimulated for 1hr with TNF (100ng/ml) before the assay. After activation, bEND3 monolayers were washed and 50ul of chemokine solutions (2x) were added. Peritoneal cells (2hr after TG) or WEHI-231 were prepared at $2x10^6$ / ml in migration medium and 50ul of cell mix was gently pipetted on bEND3 layer and incubated at 37°C for 45 minutes. Monolayers were then gently washed with migration medium (5x) and 100ul of 5mM EDTA solution was added to each well and incubated for 15 min on ice. Harvested cells were centrifuged, washed and resuspended in FACS buffer for flow cytometry analysis. To test integrin dependency, cells were inhibited with 20ug/ml of anti-aL and anti-a4 blocking antibody (BioXcell) for 15 min at 37°C before the assay. Cells and migration stimuli were diluted in 0.5% migration plus medium. Data are plotted as % of input migration.

Internalization assay

Murine and human GPR35 were cloned into an MSCV-GFP/Thy1.1 retroviral vector with an N-terminal OX56 epitope tag (Lu et al., 2019) to track surface expression levels of each receptor. Both receptors were transduced into WEHI-231 cells. Confluent cultures of each of the lines indicated above were washed twice in migration medium, resuspended at 5×10^6 cells ml^{-1} and resensitized at 37 °C for 10 min. For each line, 50 μl of cells was aliquoted into a 96-well plate. Stimuli were prepared in migration medium and 50-μl aliquots were placed into a 96-well round bottom plate that was placed in a 37 °C cell culture incubator for 45 min. The plate was then placed on ice, washed with ice-cold flow cytometry buffer and stained for OX56 by flow cytometry. OX56 surface levels on transduced cells were assessed by gating on the top 40% of OX56-expressing cells in the control condition, then using the same gate on the transduced cells treated with various compounds to assess % internalization.

Platelet and mast cell purification and activation and 5-HIAA ELISA

Blood from control or treated (Phenelzine or Fluoxetine) mice was drawn from the inferior vena cava into a syringe containing acid citrate dextrose (Sigma Aldrich C3821). Platelet-rich plasma was obtained by mixing blood with modified HEPES-Tyrode's buffer (140mM NaCl, 2mM KCl, 12mM NaHCO3, 0.3mM NaH2PO4, 1mM MgCl2, 5.5 mM glucose, 5mM HEPES, pH6.8) containing 0.35% BSA followed by 300g centrifugation during 4 min. PGI2 was added to platelet-rich plasma (500nM final concentration) and platelets were then pelleted by centrifugation at 1000g for 6 min. Pelleted platelets were resuspended in modified HEPES-Tyrode's buffer (pH 7.38) containing ADP scavenger apyrase (adenosine-5'-triphosphate diphosphohydrolase, 0.02 IU/ml final) before being put at rest for 45 min at 37°C. Platelets were activated with 0.5 IU/mL of Thrombin for 3 minutes at 37°C, centrifugated and supernatant was collected for further experiments. All reagents were purchased from Sigma, except BSA (RPI research product international). Mast cells were isolated from peritoneal lavage of B6 mice by positive selection (EasySep Mouse CD117 (cKIT) Positive Selection Kit). P815 cells or isolated primary mast cells were diluted in migration medium and seeded in flat 24 well plates ($5x10^5$ cells / well) 30 min before activation with LPS (100ng/ml, Sigma). Supernatants were collected 2hr after activation, centrifuged at 10000 rpm for 30min at 4°C and tested for migration or ELISA. To quantify 5-HIAA in cell supernatants, Mouse 5-Hydroxyindoleacetic acid (5-HIAA) ELISA Kit (AssayGenie) was used following manufacturer instructions.

Intravital imaging

Intravital imaging of omentum was performed as previously described (Buscher et al., 2016). Briefly, mice were anesthetized with 5% isoflurane (Low-Flow Anesthesia System, Somno Suite®) at 1.5 hr after TG injection. Follow-up surgery and imaging was carried out with lower concentrations of isoflurane (between 0.5% and 0.8%, adjusted according to breathing rate). After removal of abdominal fur, a 1–1.5-cm median incision was done at the linea alba of the upper abdomen to exteriorize the greater omentum, gently handed with cotton-wool tips. A custom-made microscopic stage allowed fixation of the omentum between two cover slips, immersed in warm saline. Throughout the experiment the animals were kept warm on a 37 °C heating pad (Biogenics). To visualize neutrophils and vessels in mixed chimeras, PE-conjugated anti–mouse Ly6G (2ug/200ul, #127608, Biolegend) and dextran Cascade Blue (#D1976, Fisher) were injected i.v. immediately before surgery. For transfer experiments, BM-derived neutrophils were enriched (purity > %80) with negative magnetic selection (EasySep™) following manufacture instructions and using the following biotin-conjugated antibodies: rat anti-mouse anti-CD115 (CSF-IR, #135508), anti-SiglecF (S17007L, #155512), anti-CD3 (145-2C11, #100304, BioLegend), anti-B220 (RA3-6B2, #103204, BioLegend), anti-CD4 (GK1.5, #100404, Biolegend), anti-CD8 (53-6.7, #100704, BioLegend). Purified WT and KO neutrophils were stained with Cell trace Violet or CFSE (#C34554, ThermoFisher), or Deep red (#C34565, Life Tech) according to manufacture instructions and mixed 50:50 before injection (3×10^7 neutrophil / mouse in 200ul saline), 30 min before i.p. TG. Dextran Cascade Blue was used as blood tracer. Pf4Cre mTmG mice expressed GFP selectively in platelets; these mice broadly expressed tdTom in other cell types including neutrophils but the intensity of red fluorescence in these cells was weak as reported (Muzumdar et al., 2007) and was at least 100-fold less intense than for the transferred CMTMR labeled neutrophils such that only the transferred cells were detected. To image inflamed skin, mice were anesthetized with 5% isoflurane at

1.5 hr after *Listeria* ear-pricking. After hair removal, the dorsal side of the ear was attached to a plastic coverslip mounted on a 37°C heating stage. Images were acquired with a Zeiss LSM 7MP equipped with a Chameleon laser (Coherent) and a x20 objective, samples were excited at 820-850nm. For video acquisition, a series of planes of 3μm z-spacing spanning a depth of 30–60 μm were collected every 7–14 s.

Image processing and quantification

Multiphoton intravital movies were imported into IMARIS software (v.9.6.0). Vessel surface was obtained using IMARIS built-in surface function based on dextran-Cascade Blue or dextran-Rhodamine plus CD31-PE or TdTomato (mTmG) signal as indicated. To visualize WT and KO neutrophils in Mrp8-Cre^{+} mTmG / GPR35 KO mixed chimeras, we injected i.v. anti-Ly6G-PE and imaged 2 independent neutrophil populations: double-positive Mrp8-Cre^{+} mTmG (GFP^{+}) Ly6G-PE^{+} WT and single-positive Ly6G-PE^{+} GPR35 KO neutrophils. To create 2 independent channels for WT and KO neutrophils, GFP channel was subtracted from Ly6G-PE^{+} channel using channel subtraction function in IMARIS. To track single cells, surface seed points were created and tracked over time with IMARIS spot built-in function. Tracks were manually examined and verified. To quantify transmigrating tracks, an iso-surface of the vessel was generated and tracks that had a shortest distance from the surface of $\leq$ 0μm (points internal to the surface have a negative value) were selected using Imaris. Of these, tracks that left the vessel and moved at least 5μm away were manually identified and scored as transmigrating. To quantify interactions of WT or KO neutrophils with platelets, iso-surfaces representing WT / KO neutrophils and platelets were created based on channel signal intensity (Imaris). Mean duration contact of WT or KO neutrophils with platelet surfaces was quantified by using Kiss and Run Imaris built-in function. Transmigrating track shortest distance to platelets was automatically quantified after generation of platelets surfaces and tracks (Imaris).

QUANTIFICATION AND STATISTICAL ANALYSIS

Prism software (GraphPad 9.0.1) was used for all statistical analyses. The statistical tests used are specified in the figure legends. Two-tailed unpaired t-tests were performed when comparing only two groups, Paired- t-tests were used to compare internally controlled replicates, and ordinary one-way ANOVA using Turkey's multiple comparisons test was performed when comparing one variable across multiple groups. $P < 0.05$ was considered significant. In summary graphs, points indicate individual samples and horizontal lines are means or medians as indicated. In bar graphs, bars show means and error bars indicate standard error mean (SEM).

Supplemental figures

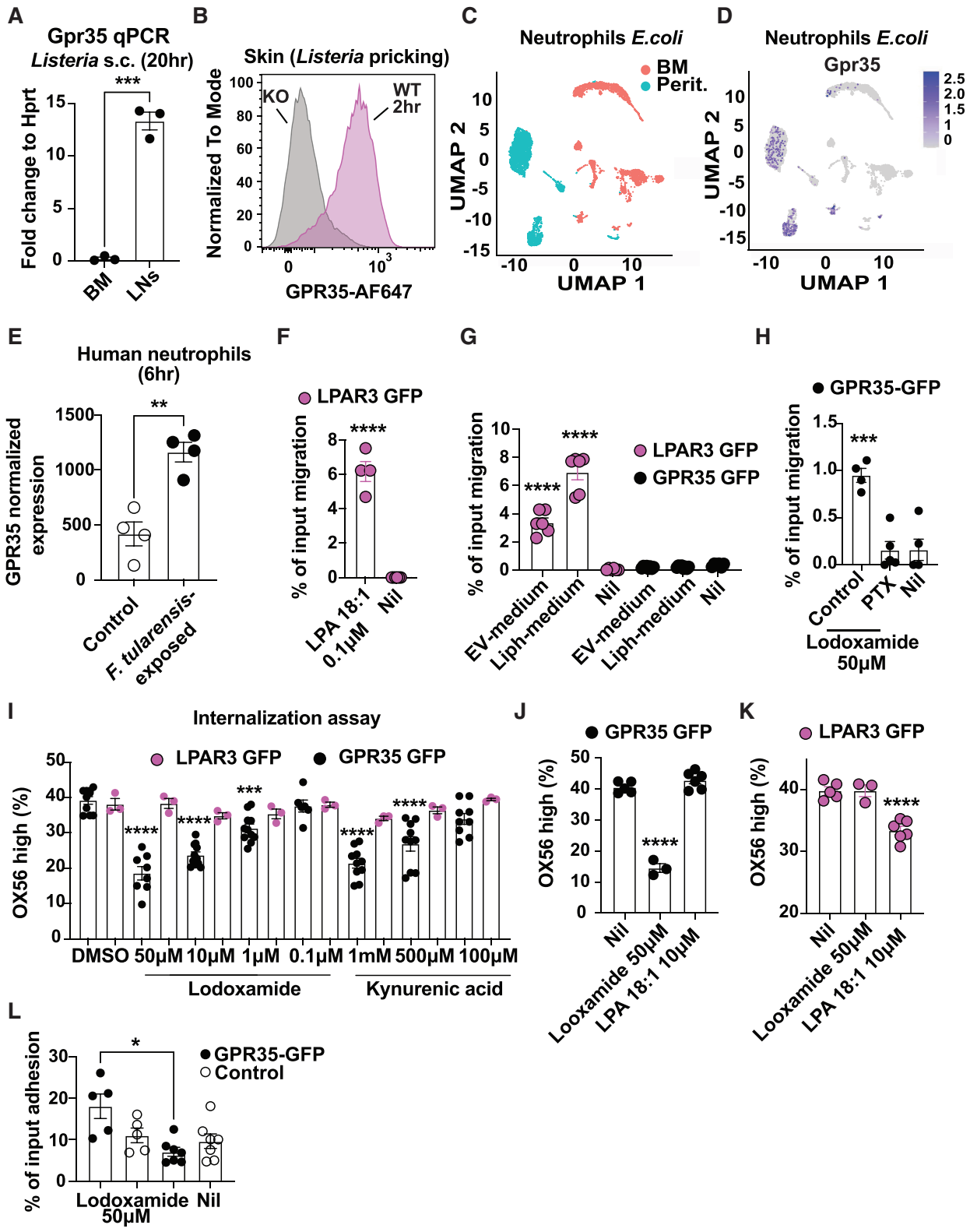

(legend on next page)

Figure S1. GPR35 expression is enhanced upon neutrophil mobilization, related to Figure 1

(A) qPCR for expression of Gpr35 (relative to Hprt) in Ly6G$^+$ Ly6C$^+$ CD11b$^+$ CXCR2$^+$ neutrophils sorted from BM or LNs 20 h after *Listeria* s.c. injection (n = 3).

(B) Intracellular flow cytometry for GPR35 in Ly6G$^+$ CD11b$^+$ Ly6C$^+$ neutrophils from ear skin 2 h after *Listeira* pricking WT or GPR35 KO mice.

(C and D) Single-cell RNA-seq UMAP plots (GSE137540) of murine peritoneal 24 h post *E. coli* injection or steady-state BM neutrophils (C) showing Gpr35 expression values (D).

(E) GPR35 normalized expression in control or *F. tularensis*-exposed (6 h) human neutrophils (E-GEOD-37416 , n = 4).

(F and G) Quantification of transwell migration of LPAR3-GFP WEHI-231 cells to 0.1 μM 1-acyl LPA 18:1 (F) (LPA, n = 4; Nil, n = 6) or to Liph-overexpressing 293T-cell culture medium as a source of 2-acyl LPA (GPR35-GFP, n = 6; LPAR3-GFP, n = 8) (G).

(H) Quantification of migration of GPR35-GFP WEHI-231 cells treated or not with pertussis toxin (PTX) to 50 μM Lodoxamide (control, n = 4; PTX, Nil, n = 5).

(I–L) Internalization assay using cells expressing OX56 epitope-tagged GPR35 or LPAR3, read-out by measuring surface OX56 levels with flow cytometry. OX56-GPR35 (black) or OX56-LPAR3 (purple) WEHI-231 cells were incubated with Lodoxamide or kynurenic acid (I), and Lodoxamide or LPA 18:1 (J and K) (I, n = 3–11, J and K, n = 3–6). (L) Quantification of adhesion assays performed with GPR35-GFP or control WEHI-231 cells. Single dots represent technical replicates. Data are pooled from two (F–H and L) and four (I–K) independent experiments. *p < 0.05, ***p < 0.001, ****p < 0.0001. Data are presented as mean ± SEM.

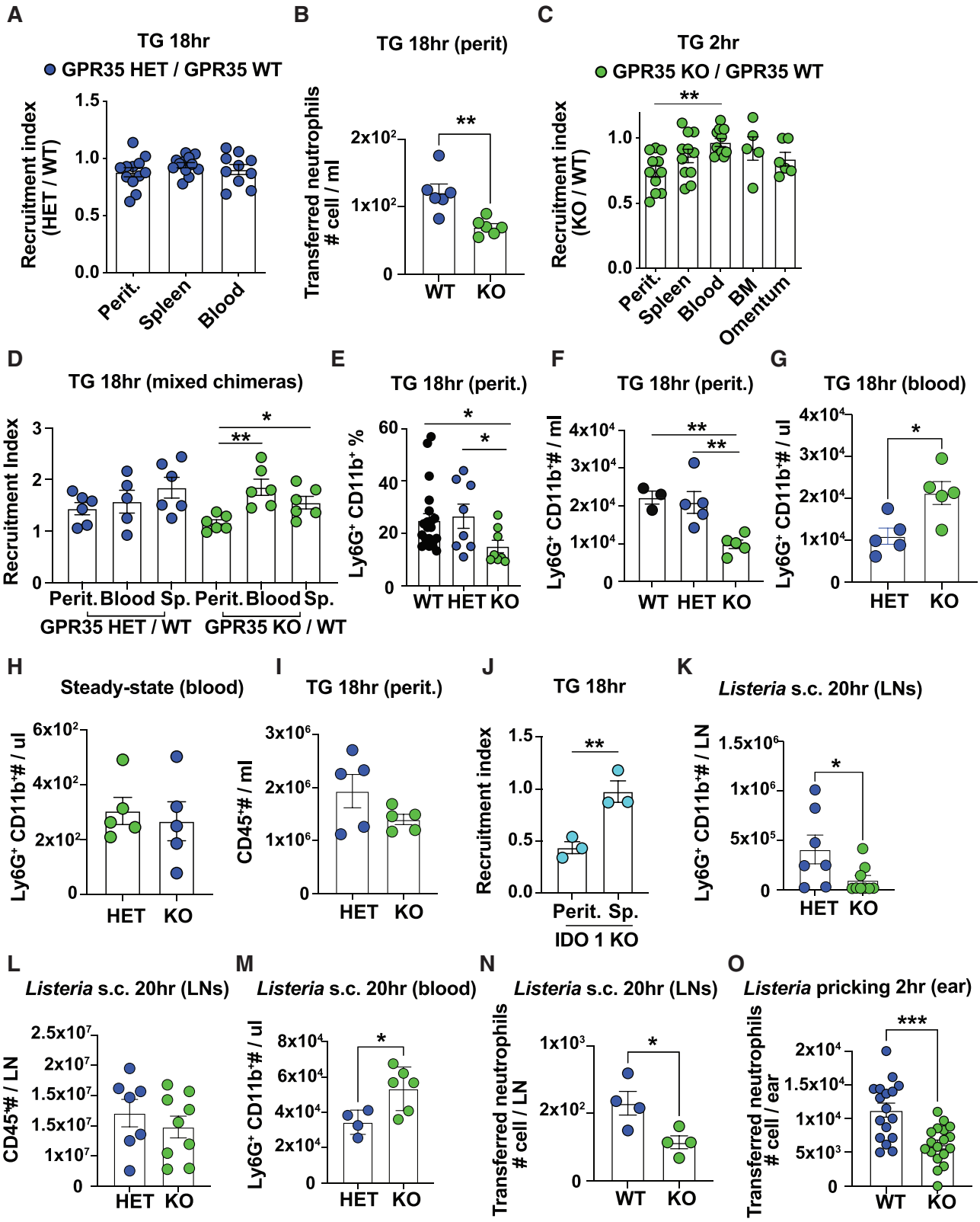

(legend on next page)

Figure S2. GPR35 enhances neutrophil homing to inflamed tissues, related to Figure 2

(A) Quantification of GPR35 HET/WT (A, peritoneum, n = 12; spleen, n = 11; blood, n = 10) transferred neutrophil recruitment index at 18 h after TG.
(B) Quantification of GPR35 WT or KO transferred neutrophil numbers at 18 h after TG (n = 6).
(C) Quantification of GPR35 KO/WT (peritoneum, spleen, blood, n = 11; BM, n = 5; omentum, n = 6) transferred neutrophil recruitment index at 2 h after TG.
(D) Quantification of neutrophil recruitment index in GPR35 HET/WT CD45.1 or KO/WT CD45.1 mixed chimeras 18 h after TG (n = 6). Note that although the BM was mixed 1:1, in some cases the chimerism favored the CD45.2 (GPR35 HET or KO) donor, giving a "recruitment index" in blood of greater than 1.
(E–I) Quantification of peritoneal $Ly6G^+$ $CD11b^+$ neutrophils percentages (E, WT, n = 11; HET, KO, n = 8) and numbers (F, WT, n = 3; HET, KO n = 5), blood $Ly6G^+$ $CD11b^+$ neutrophils numbers (G, n = 5), and endogenous peritoneal $CD45^+$ cells (I, n = 5) at 18 h after TG, or blood neutrophils numbers at steady state (H, n = 5).
(J) Quantification of transferred neutrophil recruitment index (GPR35 KO/WT) in peritoneum and spleen of IDO1 KO mice 18 h after TG (n = 3).
(K–O) Quantification of endogenous LN $Ly6G^+$ $CD11b^+$ neutrophils (K, WT, n = 7; KO, n = 9), LN $CD45^+$ cells (L, WT, n = 7; KO, n = 9), blood $Ly6G^+$ $CD11b^+$ neutrophils (M, n = 4; KO, n = 6), LN transferred neutrophils (N, n = 4), or skin transferred neutrophils (O, WT, n = 17; KO, n = 18). One-way ANOVA with Turkey post-test was applied: $^*p < 0.05$, $^{**}p < 0.005$, in (C–F). Student t test was applied in (B, G, J, K, and M–O): $^*p < 0.05$, $^{**}p < 0.005$, $^{***}p < 0.001$. Data are pooled from 5 (A and O) and two (B–K and N) independent experiments or representative of two independent experiments (I and M). Data are presented as mean ± SEM.

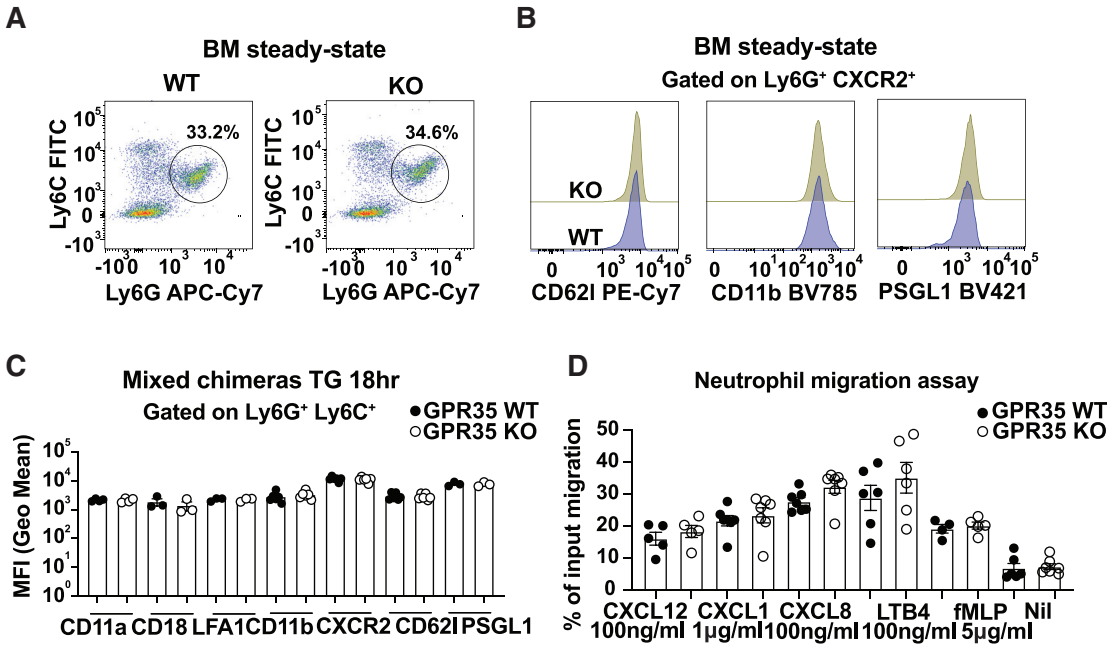

Figure S3. Numbers, surface expression markers, and migration properties are unaltered in GPR35 KO BM neutrophils, related to Figure 2

(A) Representative flow cytometry plots showing % of Ly6G$^+$ Ly6C$^+$ neutrophils in the BM of WT (top) or KO (bottom) mice at steady state.

(B) Representative flow cytometry plots showing levels of CD62 (top), PSGL1 (bottom left), and CD11b (bottom right) in Ly6G$^+$ CXCR2$^+$ neutrophils from BM at steady state.

(C) Quantification of CD11a, CD18, LFA1, CD11b, CXCR2, CD62l, and PSGL1 MFI in Ly6G$^+$ Ly6C$^+$ peritoneal neutrophils from GPR35 KO/WT mixed chimeras at 18 h after TG (n = 3–6).

(D) Quantification of WT or KO BM neutrophil migration to CXCL12, CXCL1, CXCL8, LTB4, or fMLP at the indicated concentrations (n = 5–7). Graphs depict bars with mean ± SEM. Single dots represent biological replicates. Data are presented as mean ± SEM.

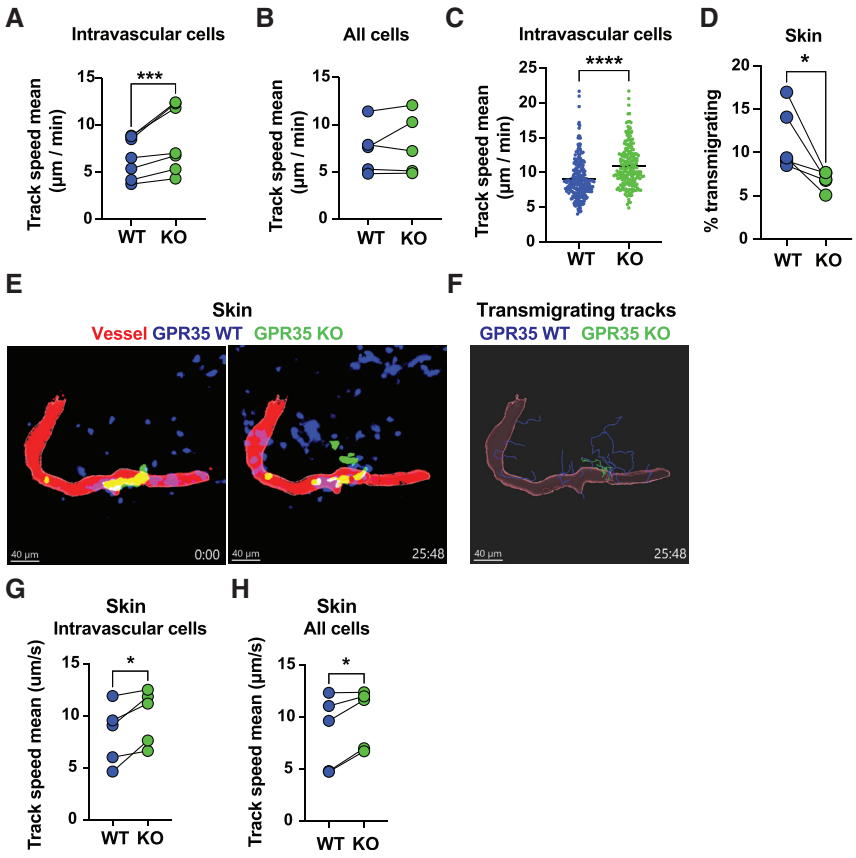

Figure S4. GPR35 sustains *in vivo* neutrophil transendothelial migration, related to Figure 3

(A and B) Quantification of track speed mean of intravascular (A) or total (B) WT and GPR35 KO neutrophils from movies of the type shown in Video S1 (n = 6) using chimeric mice of the type in Figure 3C. Single dots represent independent movies.

(C) Quantification of intravascular WT or GPR35 KO neutrophil track speed mean from Video S1 (WT, n = 238; KO, n = 217). Single dots represent independent tracks. Data are representative of six independent movies.

(D) Quantification of WT or KO transmigrating track % in the ear skin, 2 h after *Listeria* pricking (n = 5).

(E and F) Multiphoton intravital micrographs of Mrp8-Cre^{+} mTmG (blue) or GPR35 KO (green) Ly6G^{+} neutrophil transmigrating tracks from dextran-labeled vessel (red) into skin parenchyma, 2 h after *Listeria* pricking (Video S4). Image is representative of five independent movies. Time 0:00 min (left) and 25:48 min (right) (E). Vessel surface was depicted based on dextran Cascade Blue signal (F).

(G and H) Quantification of track speed mean of intravascular (G) or total (H) WT and GPR35 KO neutrophils, 2 h after *Listeria* pricking (n = 5). Single dots represent independent movies. *$p < 0.05$, ***$p < 0.001$. Data are presented as mean ± SEM.

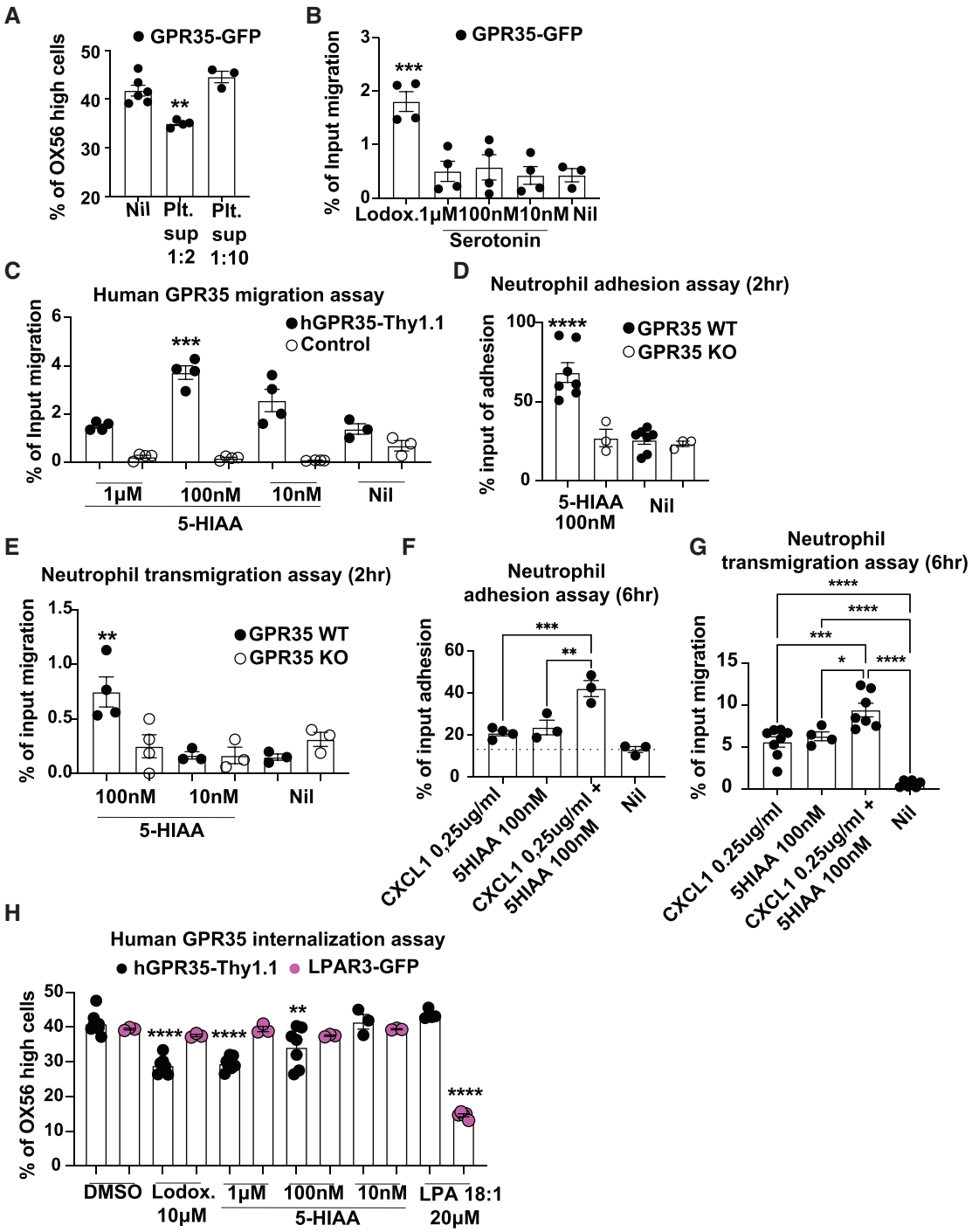

Figure S5. 5-HIAA is a ligand for murine and human GPR35 and drives *in vitro* GPR35-dependent neutrophil adhesion and transmigration, related to Figure 4

(A) Quantification of OX56 surface levels in OX56-GPR35 WEHI-231 cells incubated with activated platelet culture supernatants (Nil, n = 6; platelet sup. 1:2, n = 4; platelet sup. 1:10, n = 3).

(B) Graph showing quantification of GPR35-GFP WEHI-231 cell transwell migration to Lodoxamide and serotonin at indicated concentrations (n = 3–4). Data are pooled from 2 experiments.

(C–E) Graph showing quantification of human GPR35-Thy1.1 WEHI-231 cell transwell migration (C) (n = 3–4) or peritoneal WT (black) or GPR35 KO (white) neutrophil adhesion (D) (n = 3–7) or transmigration (E) (n = 3–4) to 5-HIAA at the indicated concentrations.

(legend continued on next page)

(F and G) Graph showing quantification of peritoneal neutrophil (6 h after TG) adhesion (F) (n = 3–4) or transmigration (G) (n = 3–8) to indicated concentrations of CXCL1, 5-HIAA or both. Data are pooled from two independent experiments.
(H) Quantification of OX56 levels in human OX56-GPR35 and OX56-LPAR3 WEHI-231 cells incubated with 5-HIAA or 18:1 LPA at indicated concentrations (n = 3–9). Data are pooled from four independent experiments. *p < 0.05, **p < 0.005, ***p < 0.001, ****p < 0.0001. Data are presented as mean ± SEM.

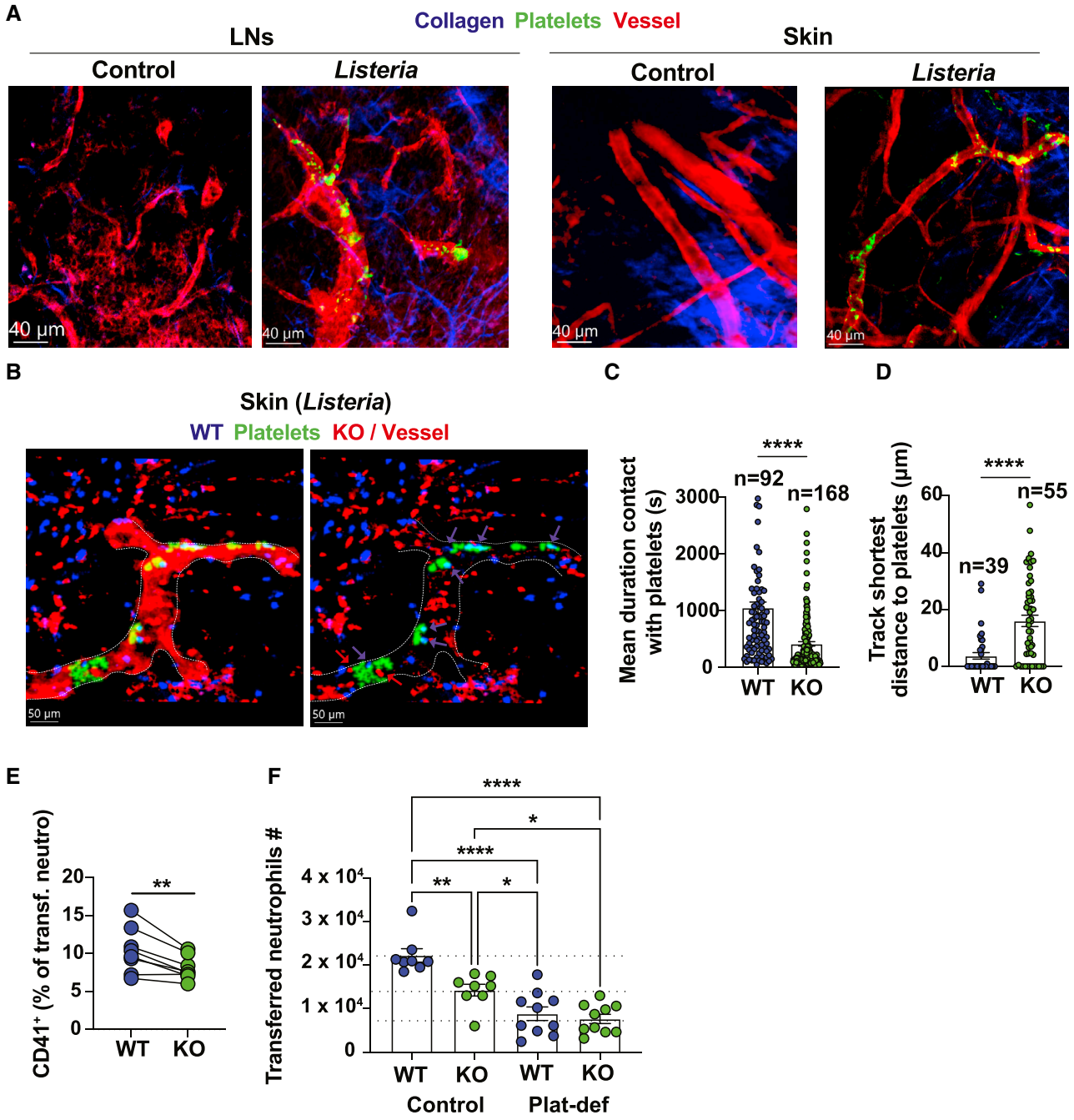

Figure S6. Activated platelets promote GPR35-dependent transmigration, related to Figure 5

(A) Multiphoton micrographs of control or *Listeria*-inflamed LNs (left, 8 h after *Listeria*) or skin (right, 2 h after *Listeria*) of Pf4-Cre × mTmG mice (collagen, blue; platelets, green; vessels, red). Images are representative of two independent experiments.

(B) Multiphoton micrograph of WT (blue) or GPR35 KO (red) transferred neutrophils in skin of Pf4-Cre × mTmG mice (platelets, green; vessels, magenta). Image on left shows vessel highlighted in magenta based on maximum intensity detection of mT (membrane tdTom) signal in vessel region and dashed line in both images shows vessel boundary. Blue and red arrows point to WT and GPR35 KO neutrophils, respectively, that are in contact with platelet clusters (in cases where blue [WT] neutrophils fully overlap with GFP$^+$ clusters they appear cyan).

(C and D) Quantification of mean duration contact with platelets of intravascular WT (n = 92) or GPR35 KO (n = 168) neutrophils (C, Video S5) and WT (n = 39) or KO (n = 55) transmigrating track shortest distance to platelets (D). Cells were injected at a ratio of 3:1 (KO:WT) to increase the number of transmigrating KO cells. Data are representative of five independent movies (C) or pooled from two representative movies (D). Single dots represent single cells.

(legend continued on next page)

(E) Quantification of data shown in Figure 5D (n = 8) showing % of CD41$^+$ WT or KO transferred neutrophils in blood 2 h after TG. Single dots represent biological replicates. Paired t test was applied: **p < 0.005. Data are pooled from two independent experiments.
(F) Quantification of transferred neutrophils numbers in control or platelet-deficient mouse skin 2 h after *Listeria* skin pricking (n = 8–10). Data are pooled from two independent experiments. *p < 0.05, ***p < 0.001, ****p < 0.0001. Data are presented as mean ± SEM.

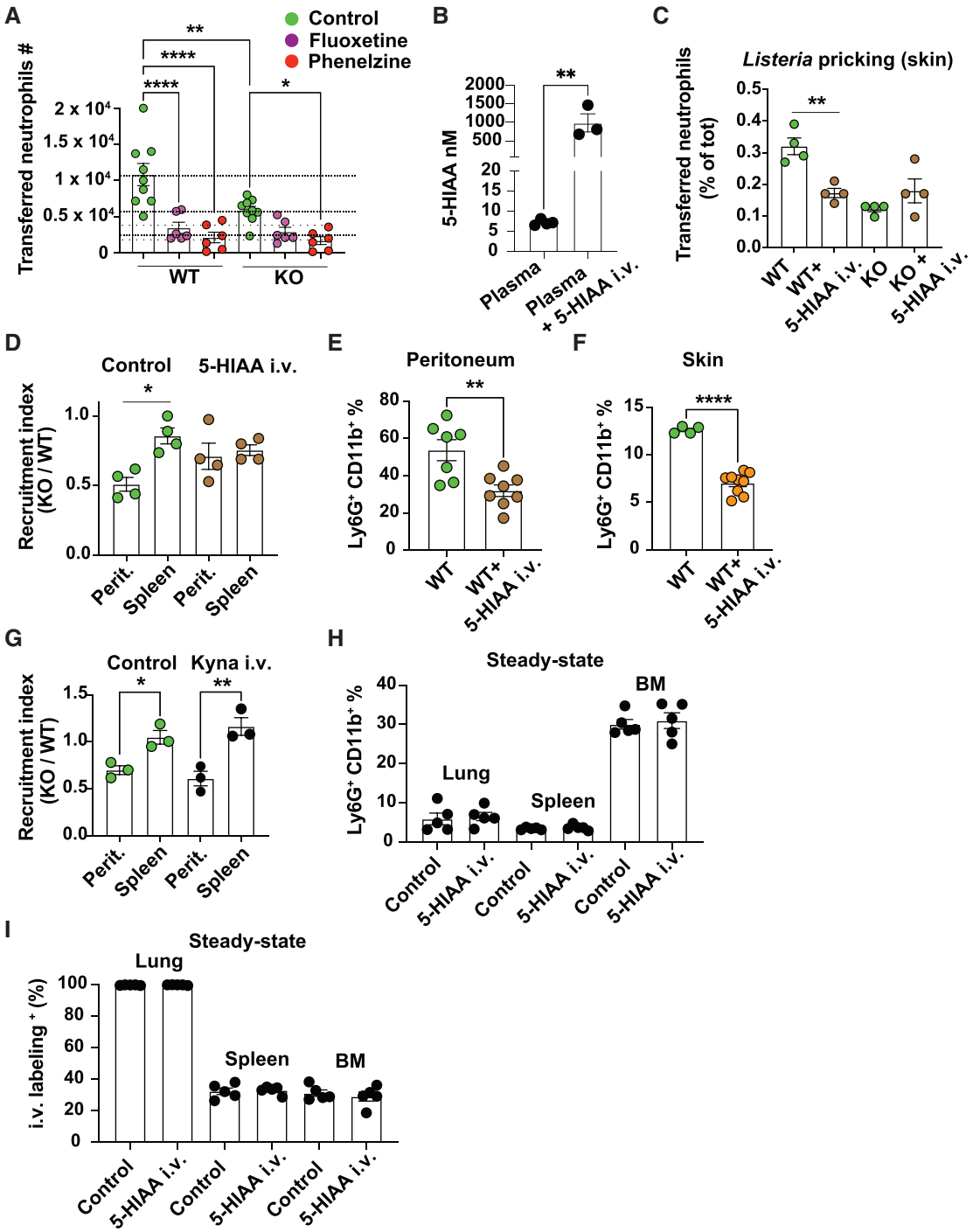

Figure S7. 5-HIAA promotes neutrophil recruitment *in vivo*, related to Figure 7

(A) Quantification of skin transferred WT and KO neutrophil numbers in mice treated with fluoxetine of phenelzine 2 h after *Listeria* skin pricking (n = 6–9).

(B) ELISA quantification of 5-HIAA in plasma from control mice and mice treated i.v. with 5-HIAA 2 h earlier. Graph depicts bars with mean ± SEM.

(C–E) Quantification of transferred neutrophil % (C, n = 4), recruitment index (D, n = 4), and endogenous neutrophil % (E) (WT, n = 7; KO, n = 8) in the peritoneum of mice 2 h after i.p. TNF treatment or in the skin 2 h after *Listeria* pricking in mice treated with i.v. 5-HIAA. Graphs depict bars with mean ± SEM; single dots represent biological replicates. One-way ANOVA with Turkey post-test was applied: *$p < 0.05$, **$p < 0.005$, ****$p < 0.0001$. Data are pooled from two independent experiments (A) or representative of two independent experiments (B–E).

(F) Quantification of $Ly6G^+$ $CD11b^+$ endogenous neutrophil % in skin 2 h after *Listeria* pricking in mice treated with i.v. 5-HIAA (WT, n = 4; KO, n = 9). Data are pooled from two independent experiments.

(legend continued on next page)

(G) Quantification of neutrophil recruitment index in peritoneum and spleen of mice treated with i.v. kynurenic acid 2 h after i.p.TNF treatment (n = 3). Data are representative of two independent experiments. Single dots represent biological replicates. *$p < 0.05$, **$p < 0.005$.
(H and I) Graph showing quantification of $Ly6G^+$ $CD11b^+$ endogenous cells (H, n = 5) or % of CD45-PE^+ intravascular cells within $Ly6G^+$ $CD11b^+$ cells (I, n = 5) in lungs, spleens, and BM of mice treated i.v. 2 h before with saline (control) or 5-HIAA. Data are presented as mean ± SEM.

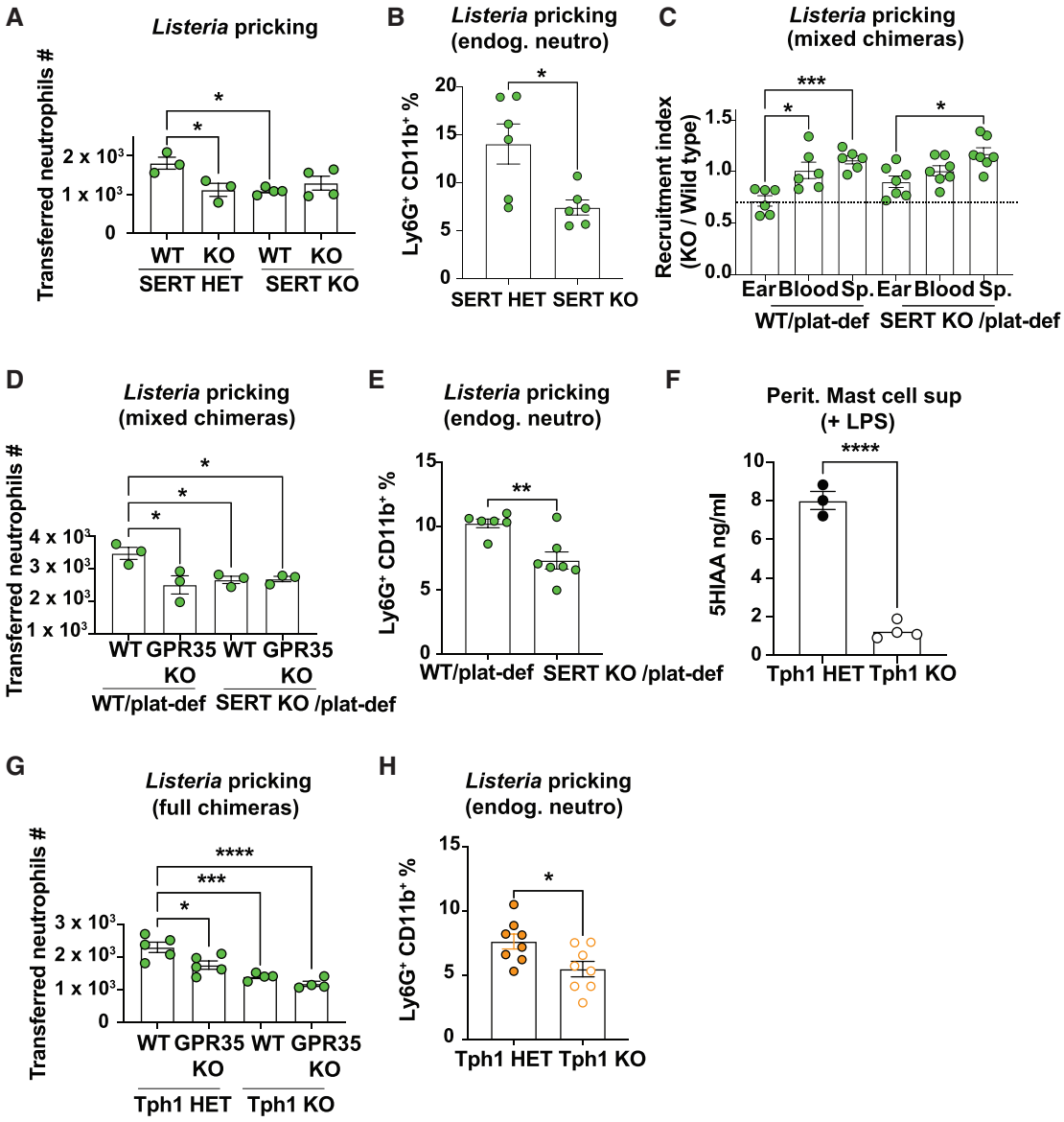

Figure S8. GPR35-driven recruitment is impaired in mice lacking SERT or Tph1, related to Figure 7

(A and B) Quantification of transferred neutrophils numbers (A, n = 3–4) and endogenous Ly6G$^+$ CD11b$^+$ neutrophil percentages (B, n = 6) in SERT HET or KO mice 2 h after *Listeria* skin pricking.

(C–E) Quantification of transferred neutrophil recruitment index (C, n = 6–7), transferred neutrophil numbers (D, n = 3), and endogenous Ly6G$^+$ CD11b$^+$ neutrophil percentages (E, n = 6–7) in WT/platelet-deficient or SERT KO/platelet-deficient mixed chimeras at 2 h after *Listeria* skin pricking.

(F) Graph showing ELISA quantification of 5-HIAA in culture supernatants of LPS stimulated peritoneal mast cells from Tph1 HET or KO BM chimeras (n = 3–4). Single dots represent biological replicates.

(G and H) Quantification of transferred neutrophil numbers (G, n = 4–5) and endogenous Ly6G$^+$ CD11b$^+$ neutrophil percentages (H, n = 8) in Tph1 HET or KO full chimeras at 2 h after *Listeria* skin pricking. Data in (A, D, and G) are representative of two independent experiments; data in (B, C, E, and H) are pooled from two independent experiments. *p < 0.05, **p < 0.005, ***p < 0.001, ****p < 0.0001. Data are presented as mean ± SEM.